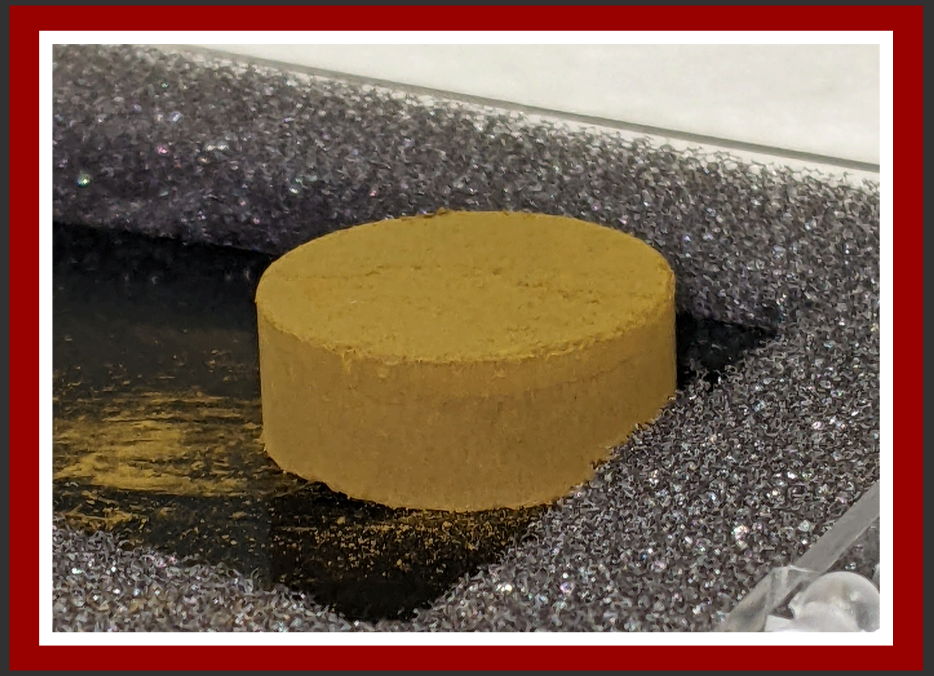

Searching for Exotic Polarized-Electron Polarized-Neutron Interactions in Polycrystalline Terbium Iron Garnet Using Slow Neutron Polarimetry

Krystyna Lopez

INDIANA UNIVERSITY BLOOMINGTON

PSTP 2024

20TH INTERNATIONAL WORKSHOP ON POLARIZED SOURCES, TARGETS, AND POLARIMETRY

SEPT. 22-27 | JEFFERSON LAB, NEWPORT NEWS, VA

Outline

- Theoretical Motivation
- Why Ferrimagnets?
- TbIG@HFIR2023
- TbIG@HFIR2024
- Future Work

Why Exotic Force Searches?

Strong CP problem says QCD should violate CP symmetry, but highly suppressed

Peccei and Quinn proposed new (broken) symmetry — Moody and Wilczek proposed potentials based on “axion”, where potentials depend on spin of one or both particles

Many experiments are conducted to search for new possible interactions

“Typical approaches include torsion pendulums, torsional oscillators, atomic magnetometers, NMR, nitrogen vacancy (NV) centers in diamond, magnetic microscopes, **polarized neutron experiments**, measurements of atomic and molecular EDMs” [1]

Dark matter can induce spin-dependent neutron-matter interactions [2]

[1] K. Wei, *et al.* Nat. Commun. **13**, 7387 (2022)
[2] A. Costantino, *et al.* J. High Energ. Phys. **2020**, 148 (2020)

Spin-Dependent Potentials

Dobrescu and Mocioiu expand:

- Single particle exchange of:
  - Spin-0 boson (m>0)
  - Spin-1 boson (m=0)
  - Spin-1 boson (m>0)
- non-relativistic limit (v << c)
- rotationally-invariant

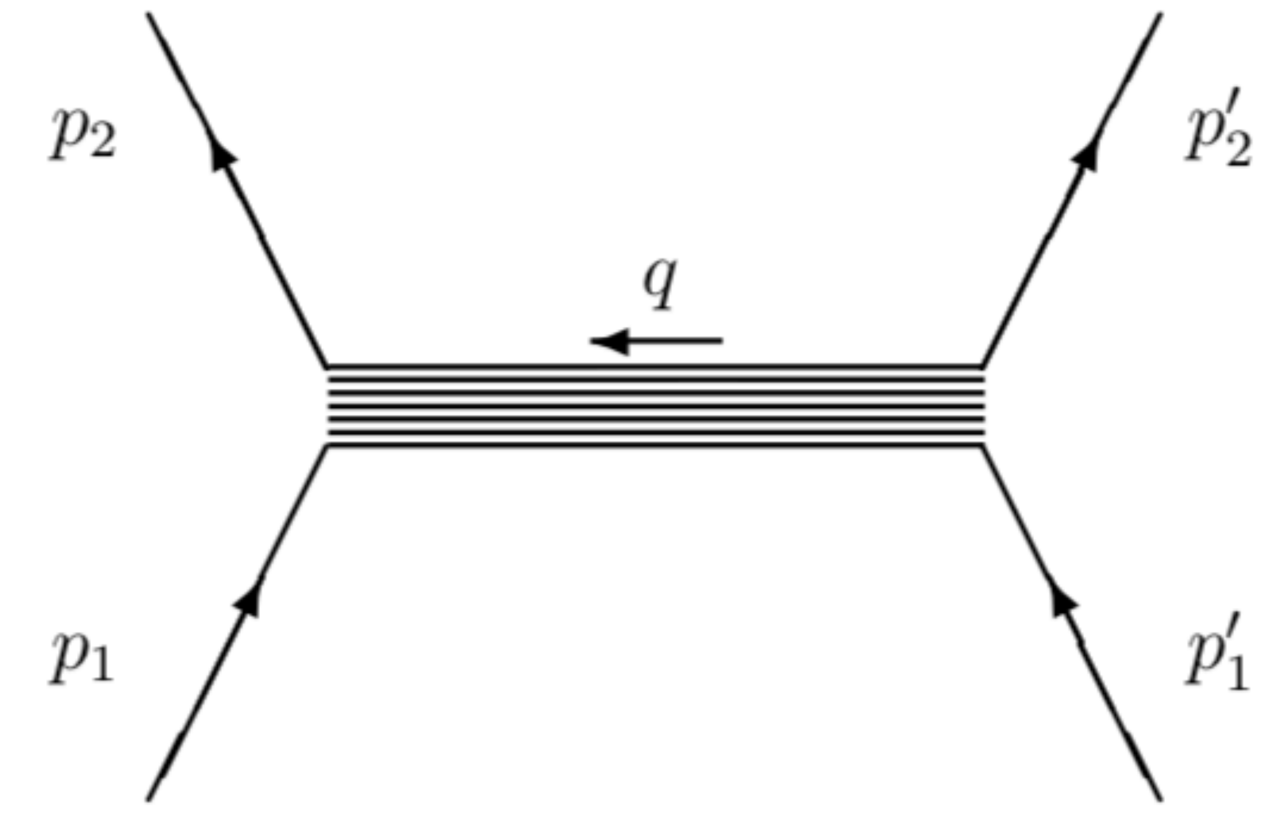

Figure 1: Elastic scattering of two fermions mediated by some very light particles represented generically by the horizontal blob of four-momentum q.

B. Dobrescu and I. Mocioiu, J. High Energy Phys. 0611, 005 (2006)

Results in:

- 16 combinations of spin/momentum
- 72 Independent couplings $f_i^{1,2}$
  - i = 1-16
  - 1,2 = e, p, n, etc.

Spin-Dependent Potentials

B. Dobrescu and I. Mocioiu, J. High Energy Phys. 0611, 005 (2006)

$$V_2 = f_2^{ee}\frac{\hbar c}{4\pi}(\hat\sigma_1\cdot\hat\sigma_2)\left(\frac{1}{r}\right)e^{-r/\lambda}$$

$$V_3 = f_3^{ee}\frac{\hbar^3}{4\pi m_e^2 c}\left[(\hat\sigma_1\cdot\hat\sigma_2)\left(\frac{1}{\lambda r^2}+\frac{1}{r^3}\right)-(\hat\sigma_1\cdot\hat r)(\hat\sigma_2\cdot\hat r)\left(\frac{1}{\lambda^2 r}+\frac{3}{\lambda r^2}+\frac{3}{r^3}\right)\right]e^{-r/\lambda}$$

$$V_{11} = -f_{11}^{ee}\frac{\hbar^2}{4\pi m_e}[(\hat\sigma_1\times\hat\sigma_2)\cdot\hat r]\left(\frac{1}{\lambda r}+\frac{1}{r^2}\right)e^{-r/\lambda}$$

"Static" spin-spin interactions

$$V_{6+7} = -f_{6+7}^{ee}\frac{\hbar^2}{4\pi m_e c}[(\hat\sigma_1\cdot\vec v)(\hat\sigma_2\cdot\hat r)]\left(\frac{1}{\lambda r}+\frac{1}{r^2}\right)e^{-r/\lambda}$$

$$V_8 = f_8^{ee}\frac{\hbar}{4\pi c}[(\hat\sigma_1\cdot\vec v)(\hat\sigma_2\cdot\vec v)]\left(\frac{1}{r}\right)e^{-r/\lambda}$$

$$V_{14} = f_{14}^{ee}\frac{\hbar}{4\pi}[(\hat\sigma_1\times\hat\sigma_2)\cdot\vec v]\left(\frac{1}{r}\right)e^{-r/\lambda}$$

$$V_{15} = -f_{15}^{ee}\frac{\hbar^3}{8\pi m_e^2 c^2}\{[\hat\sigma_1\cdot(\vec v\times\hat r)](\hat\sigma_2\cdot\hat r)+(\hat\sigma_1\cdot\hat r)[\hat\sigma_2\cdot(\vec v\times\hat r)]\}\left(\frac{1}{\lambda^2 r}+\frac{3}{\lambda r^2}+\frac{3}{r^3}\right)e^{-r/\lambda}$$

$$V_{16} = -f_{16}^{ee}\frac{\hbar^2}{8\pi m_e c^2}\{[\hat\sigma_1\cdot(\vec v\times\hat r)](\hat\sigma_2\cdot\vec v)+(\hat\sigma_1\cdot\vec v)[\hat\sigma_2\cdot(\vec v\times\hat r)]\}\left(\frac{1}{\lambda r}+\frac{1}{r^2}\right)e^{-r/\lambda}$$

Velocity-dependent spin-spin interactions

$$V_{4+5} = -Z\left[f_\perp^{ee}+f_\perp^{ep}+\left(\frac{A-Z}{Z}\right)f_\perp^{en}\right]\frac{\hbar^2}{8\pi m_e c}[\hat\sigma_1\cdot(\vec v\times\hat r)]\left(\frac{1}{\lambda r}+\frac{1}{r^2}\right)e^{-r/\lambda}$$

$$V_{9+10} = Z\left[f_r^{ee}+f_r^{ep}+\left(\frac{A-Z}{Z}\right)f_r^{en}\right]\frac{\hbar^2}{8\pi m_e}(\hat\sigma_1\cdot\hat r)\left(\frac{1}{\lambda r}+\frac{1}{r^2}\right)e^{-r/\lambda}$$

$$V_{12+13} = Z\left[f_v^{ee}+f_v^{ep}+\left(\frac{A-Z}{Z}\right)f_v^{en}\right]\frac{\hbar}{8\pi}(\hat\sigma_1\cdot\vec v)\left(\frac{1}{r}\right)e^{-r/\lambda}$$

Spin-Mass Interactions

Sensitive potentials to our ferrimagnetic target:

$$V_2 \propto (\hat\sigma_1\cdot\hat\sigma_2)$$

$$V_{12+13} \propto (\hat\sigma_1\cdot\vec v)$$

- ✓ Well constrained by H. Yan and W. M. Snow, Phys. Rev. Lett. **110** (2013)

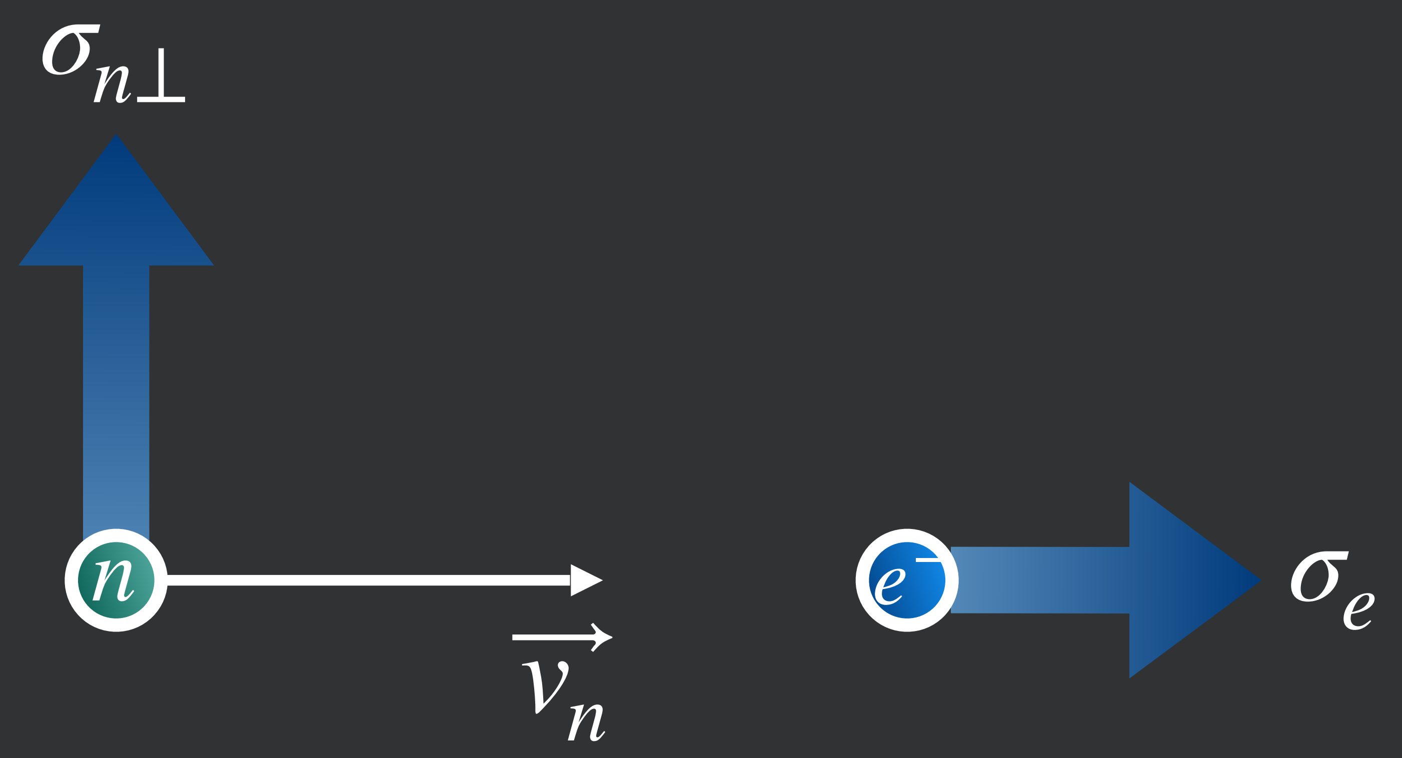

Spin-Dependent Potentials

B. Dobrescu and I. Mocioiu, J. High Energy Phys. 0611, 005 (2006)

$$V_2 = f_2^{ee} \frac{\hbar c}{4\pi} (\hat{\sigma}_1 \cdot \hat{\sigma}_2) \left(\frac{1}{r}\right) e^{-r/\lambda}$$

$$V_3 = f_3^{ee} \frac{\hbar^3}{4\pi m_e^2 c} \left[(\hat{\sigma}_1 \cdot \hat{\sigma}_2) \left(\frac{1}{\lambda r^2} + \frac{1}{r^3}\right) - (\hat{\sigma}_1 \cdot \hat{r})(\hat{\sigma}_2 \cdot \hat{r}) \left(\frac{1}{\lambda^2 r} + \frac{3}{\lambda r^2} + \frac{3}{r^3}\right) \right] e^{-r/\lambda}$$

$$V_{11} = -f_{11}^{ee} \frac{\hbar^2}{4\pi m_e} [(\hat{\sigma}_1 \times \hat{\sigma}_2) \cdot \hat{r}] \left(\frac{1}{\lambda r} + \frac{1}{r^2}\right) e^{-r/\lambda}$$

"Static" spin-spin interactions

$$V_{6+7} = -f_{6+7}^{ee} \frac{\hbar^2}{4\pi m_e c} [(\hat{\sigma}_1 \cdot \vec{v})(\hat{\sigma}_2 \cdot \hat{r})] \left(\frac{1}{\lambda r} + \frac{1}{r^2}\right) e^{-r/\lambda}$$

$$V_8 = f_8^{ee} \frac{\hbar}{4\pi c} [(\hat{\sigma}_1 \cdot \vec{v})(\hat{\sigma}_2 \cdot \vec{v})] \left(\frac{1}{r}\right) e^{-r/\lambda}$$

$$V_{14} = f_{14}^{ee} \frac{\hbar}{4\pi} [(\hat{\sigma}_1 \times \hat{\sigma}_2) \cdot \vec{v}] \left(\frac{1}{r}\right) e^{-r/\lambda}$$

$$V_{15} = -f_{15}^{ee} \frac{\hbar^3}{8\pi m_e^2 c^2} \{ [\hat{\sigma}_1 \cdot (\vec{v} \times \hat{r})](\hat{\sigma}_2 \cdot \hat{r}) + (\hat{\sigma}_1 \cdot \hat{r})[\hat{\sigma}_2 \cdot (\vec{v} \times \hat{r})] \} \left(\frac{1}{\lambda^2 r} + \frac{3}{\lambda r^2} + \frac{3}{r^3}\right) e^{-r/\lambda}$$

$$V_{16} = -f_{16}^{ee} \frac{\hbar^2}{8\pi m_e c^2} \{ [\hat{\sigma}_1 \cdot (\vec{v} \times \hat{r})](\hat{\sigma}_2 \cdot \vec{v}) + (\hat{\sigma}_1 \cdot \vec{v})[\hat{\sigma}_2 \cdot (\vec{v} \times \hat{r})] \} \left(\frac{1}{\lambda r} + \frac{1}{r^2}\right) e^{-r/\lambda}$$

Velocity-dependent spin-spin interactions

$$V_{4+5} = -Z \left[f_\perp^{ee} + f_\perp^{ep} + \left(\frac{A-Z}{Z}\right) f_\perp^{en} \right] \frac{\hbar^2}{8\pi m_e c} [\hat{\sigma}_1 \cdot (\vec{v} \times \hat{r})] \left(\frac{1}{\lambda r} + \frac{1}{r^2}\right) e^{-r/\lambda}$$

$$V_{9+10} = Z \left[f_r^{ee} + f_r^{ep} + \left(\frac{A-Z}{Z}\right) f_r^{en} \right] \frac{\hbar^2}{8\pi m_e} (\hat{\sigma}_1 \cdot \hat{r}) \left(\frac{1}{\lambda r} + \frac{1}{r^2}\right) e^{-r/\lambda}$$

$$V_{12+13} = Z \left[f_v^{ee} + f_v^{ep} + \left(\frac{A-Z}{Z}\right) f_v^{en} \right] \frac{\hbar}{8\pi} (\hat{\sigma}_1 \cdot \vec{v}) \left(\frac{1}{r}\right) e^{-r/\lambda}$$

Spin-Mass Interactions

Sensitive potentials to our ferrimagnetic target:

$$V_2 \propto (\hat{\sigma}_1 \cdot \hat{\sigma}_2)$$

$$V_{12+13} \propto (\hat{\sigma}_1 \cdot \vec{v})$$

- Well constrained by H. Yan and W. M. Snow, Phys. Rev. Lett. **110** (2013)

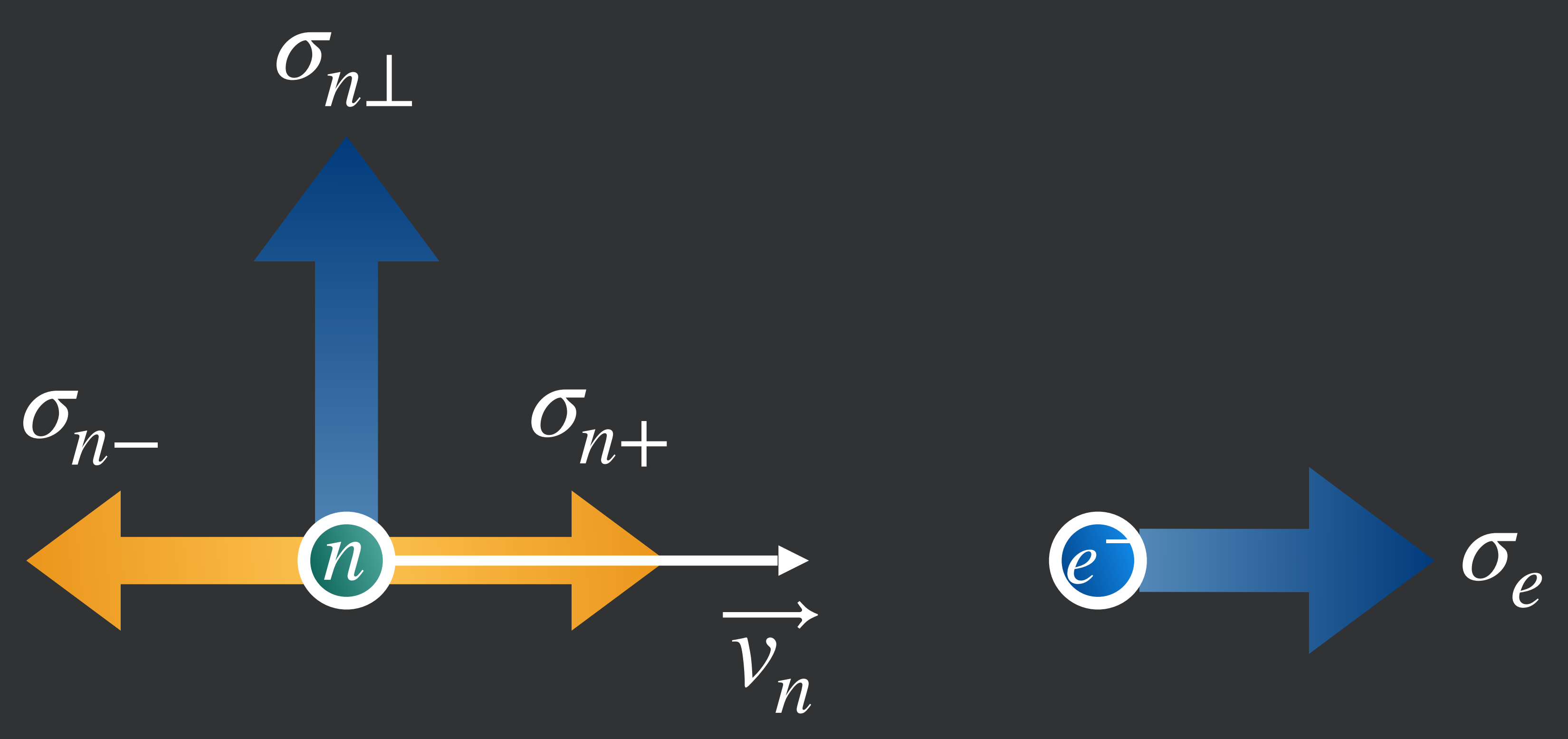

B. Dobrescu and I. Mocioiu, J. High Energy Phys. 0611, 005 (2006)

Spin-Dependent Potentials

$$V_2 = f_2^{ee}\frac{\hbar c}{4\pi}(\hat{\sigma}_1 \cdot \hat{\sigma}_2)\left(\frac{1}{r}\right)e^{-r/\lambda}$$

$$V_3 = f_3^{ee}\frac{\hbar^3}{4\pi m_e^2 c}\left[(\hat{\sigma}_1 \cdot \hat{\sigma}_2)\left(\frac{1}{\lambda r^2}+\frac{1}{r^3}\right) - (\hat{\sigma}_1 \cdot \hat{r})(\hat{\sigma}_2 \cdot \hat{r})\left(\frac{1}{\lambda^2 r}+\frac{3}{\lambda r^2}+\frac{3}{r^3}\right)\right]e^{-r/\lambda}$$

$$V_{11} = -f_{11}^{ee}\frac{\hbar^2}{4\pi m_e}[(\hat{\sigma}_1 \times \hat{\sigma}_2)\cdot \hat{r}]\left(\frac{1}{\lambda r}+\frac{1}{r^2}\right)e^{-r/\lambda}$$

"Static" spin-spin interactions

$$V_{6+7} = -f_{6+7}^{ee}\frac{\hbar^2}{4\pi m_e c}[(\hat{\sigma}_1 \cdot \vec{v})(\hat{\sigma}_2 \cdot \hat{r})]\left(\frac{1}{\lambda r}+\frac{1}{r^2}\right)e^{-r/\lambda}$$

$$V_8 = f_8^{ee}\frac{\hbar}{4\pi c}[(\hat{\sigma}_1 \cdot \vec{v})(\hat{\sigma}_2 \cdot \vec{v})]\left(\frac{1}{r}\right)e^{-r/\lambda}$$

$$V_{14} = f_{14}^{ee}\frac{\hbar}{4\pi}[(\hat{\sigma}_1 \times \hat{\sigma}_2)\cdot \vec{v}]\left(\frac{1}{r}\right)e^{-r/\lambda}$$

$$V_{15} = -f_{15}^{ee}\frac{\hbar^3}{8\pi m_e^2 c^2}\{[\hat{\sigma}_1 \cdot (\vec{v}\times\hat{r})](\hat{\sigma}_2 \cdot \hat{r}) + (\hat{\sigma}_1 \cdot \hat{r})[\hat{\sigma}_2 \cdot (\vec{v}\times\hat{r})]\}\left(\frac{1}{\lambda^2 r}+\frac{3}{\lambda r^2}+\frac{3}{r^3}\right)e^{-r/\lambda}$$

$$V_{16} = -f_{16}^{ee}\frac{\hbar^2}{8\pi m_e c^2}\{[\hat{\sigma}_1 \cdot (\vec{v}\times\hat{r})](\hat{\sigma}_2 \cdot \vec{v}) + (\hat{\sigma}_1 \cdot \vec{v})[\hat{\sigma}_2 \cdot (\vec{v}\times\hat{r})]\}\left(\frac{1}{\lambda r}+\frac{1}{r^2}\right)e^{-r/\lambda}$$

Velocity-dependent spin-spin interactions

$$V_{4+5} = -Z\left[f_\perp^{ee}+f_\perp^{ep}+\left(\frac{A-Z}{Z}\right)f_\perp^{en}\right]\frac{\hbar^2}{8\pi m_e c}[\hat{\sigma}_1 \cdot (\vec{v}\times\hat{r})]\left(\frac{1}{\lambda r}+\frac{1}{r^2}\right)e^{-r/\lambda}$$

$$V_{9+10} = Z\left[f_r^{ee}+f_r^{ep}+\left(\frac{A-Z}{Z}\right)f_r^{en}\right]\frac{\hbar^2}{8\pi m_e}(\hat{\sigma}_1 \cdot \hat{r})\left(\frac{1}{\lambda r}+\frac{1}{r^2}\right)e^{-r/\lambda}$$

$$V_{12+13} = Z\left[f_v^{ee}+f_v^{ep}+\left(\frac{A-Z}{Z}\right)f_v^{en}\right]\frac{\hbar}{8\pi}(\hat{\sigma}_1 \cdot \vec{v})\left(\frac{1}{r}\right)e^{-r/\lambda}$$

Spin-Mass Interactions

Sensitive potentials to our ferrimagnetic target:

$$V_2 \propto (\hat{\sigma}_1 \cdot \hat{\sigma}_2) \qquad V_{12+13} \propto (\hat{\sigma}_1 \cdot \vec{v})$$

- Well constrained by H. Yan and W. M. Snow, Phys. Rev. Lett. **110** (2013)

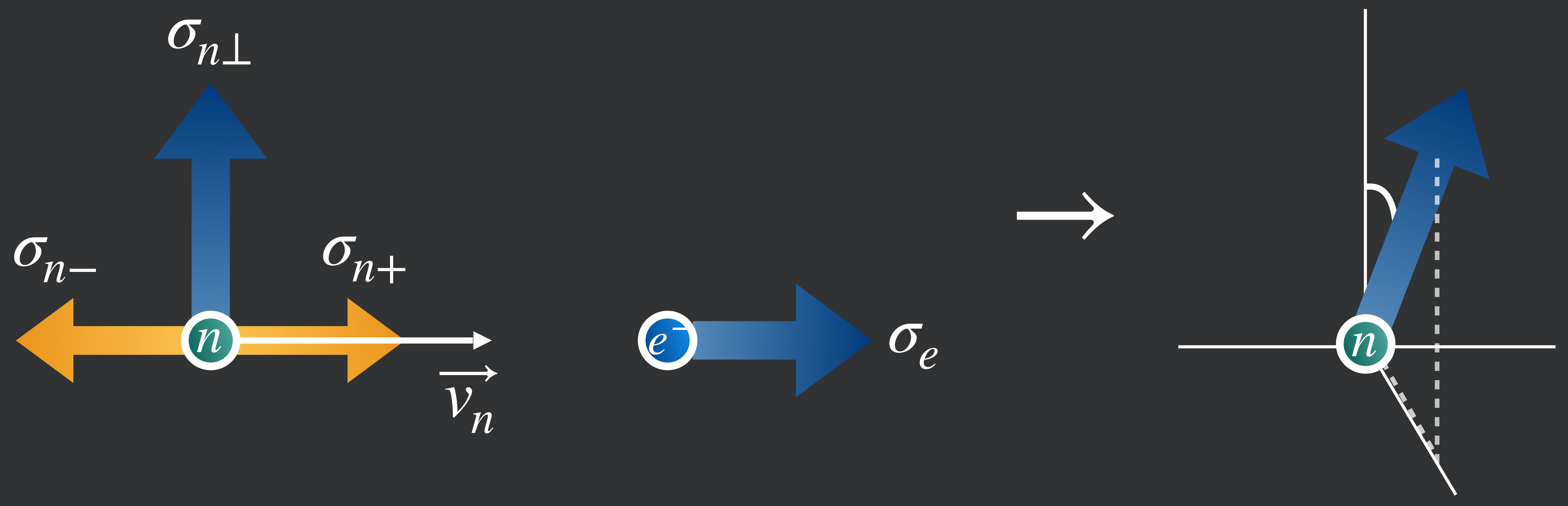

Interaction results in a transverse corkscrew of the neutron spin with rotation angle ϕ

Constraint Examples

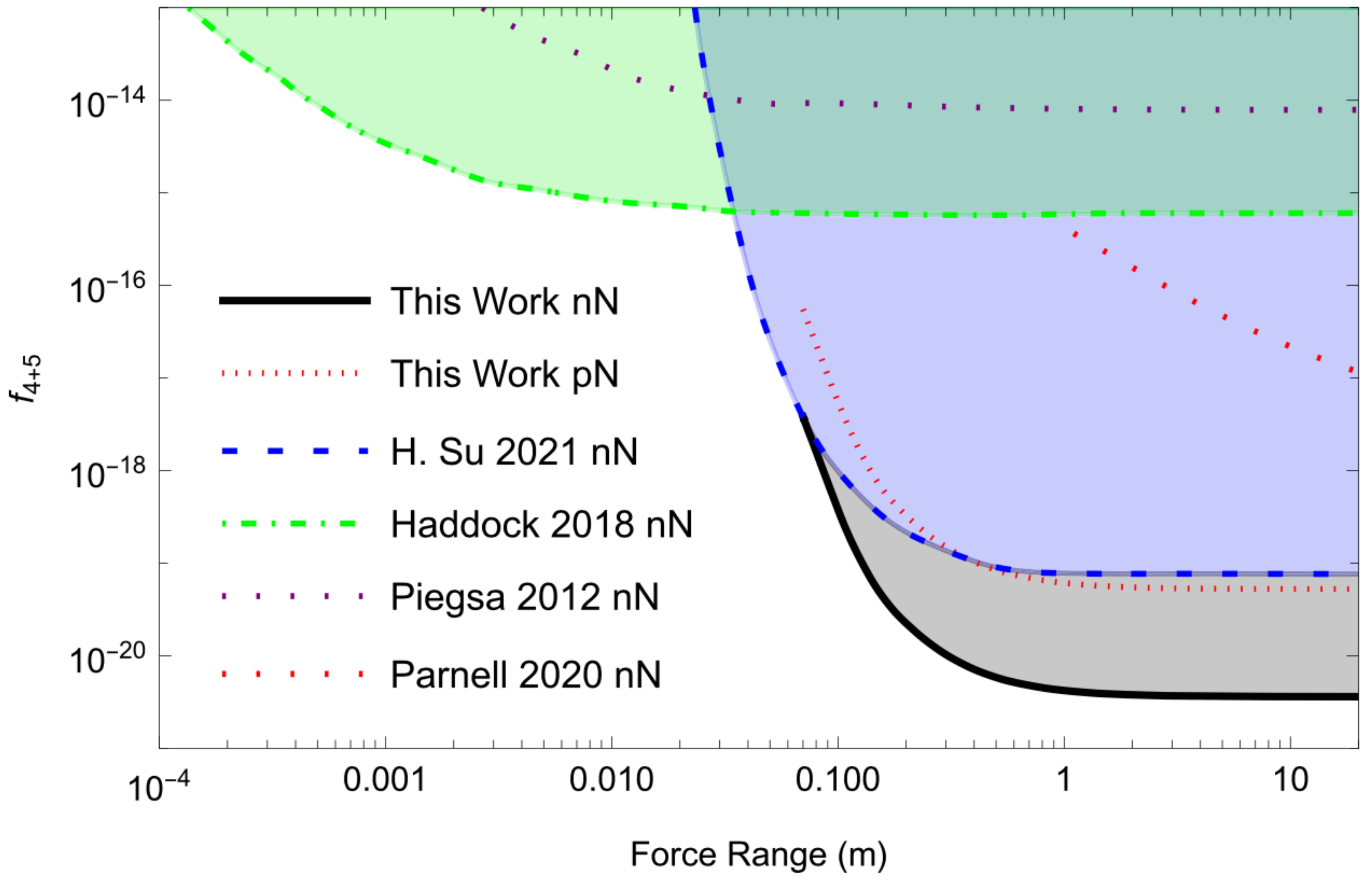

Fig. 4 | The experimental limits on f_{4+5}. The "n", "p", and "N" represent the neutron, proton, and average nucleon contribution respectively. The blue dashed line, "H.Su 2021", is from Ref. [19], the green dashed-dotted line, "Haddock 2018", is from Ref. [24], the yellow dotted line, "Piegsa 2012", is from Ref. [25], the red dashed line, "Parnell 2020", is from Ref. [50]. The black solid line and red dotted line represent our new results for "nN" and "pN" respectively.

Wei, K., Ji, W., Fu, C. *et al.* Constraints on exotic spin-velocity-dependent interactions. *Nat Commun* **13**, 7387 (2022)

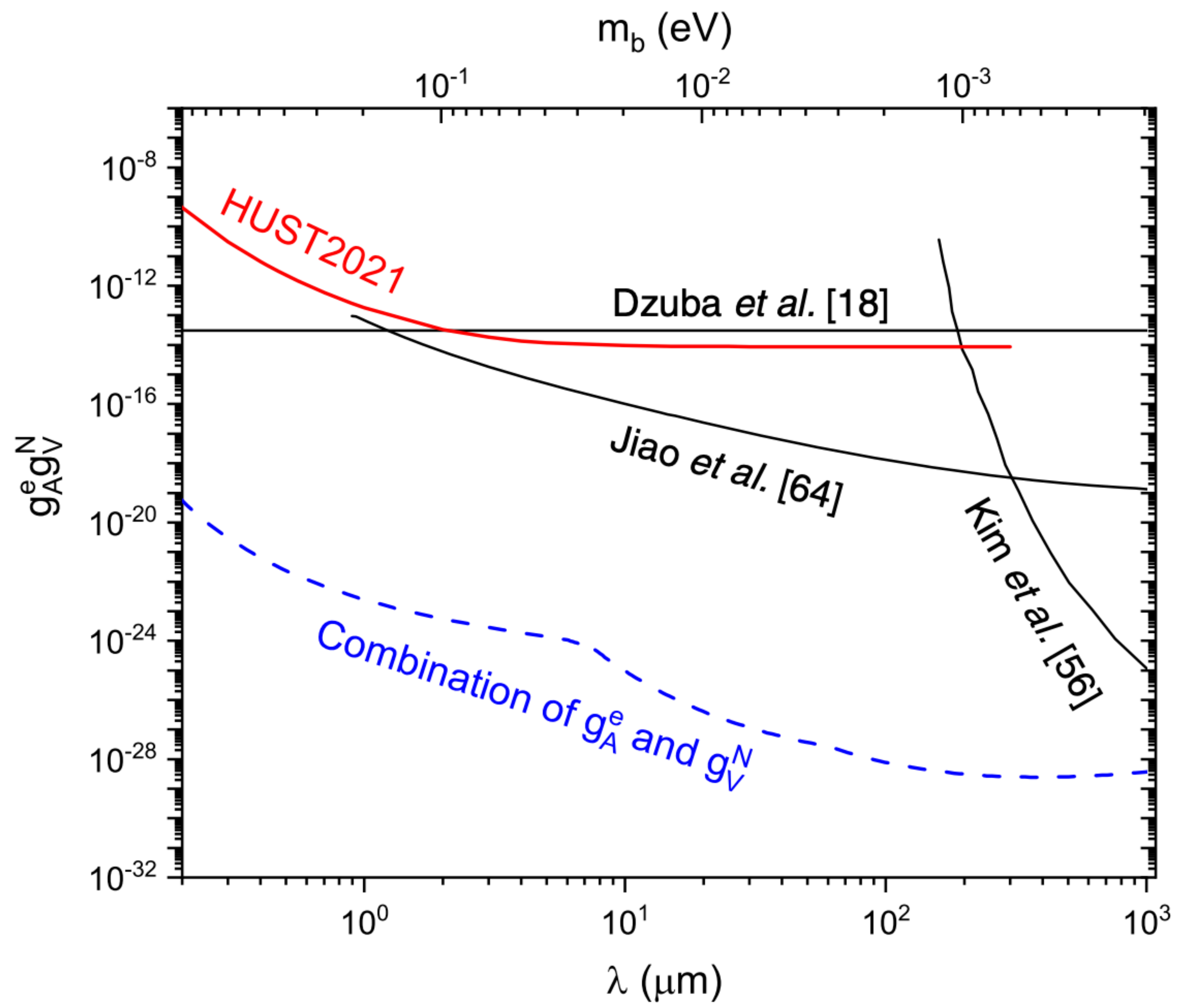

FIG. 7. Constraints on the dimensionless coupling constants $g_A^e g_V^N$ from this work as well as previous experiments [18,56,64]. The dashed line shows the limit on the combination of g_A^e and g_V^N as explained in the main text.

Ren, X., *et al.* Search for an exotic parity-odd spin- and velocity-dependent interaction using a magnetic force microscope. Phys. Rev. D **104**, 032008 (2021)

Ferrimagnets

Anti-aligned sub-moments = net moment

Ferrimagnetic moments from different ions

Ferromagnetic ↑ ↑ ↑ ↑ ↑ ↑ ↑	Below T_C, spins are aligned parallel in magnetic domains
Antiferromagnetic ↑ ↓ ↑ ↓ ↑ ↓ ↑	Below T_N, spins are aligned antiparallel in magnetic domains
Ferrimagnetic ↑ ↓ ↑ ↓ ↑ ↓ ↑	Below T_C, spins are aligned antiparallel but do not cancel

Libretexts (2021) *6.8: Ferro-, ferri- and Antiferromagnetism*, *Chemistry LibreTexts*. Libretexts. Available at: https://chem.libretexts.org/Bookshelves/Inorganic_Chemistry/Book%3A_Introduction_to_Inorganic_Chemistry_%28Wikibook%29/06%3A_Metals_and_Alloys-_Structure_Bonding_Electronic_and_Magnetic_Properties/6.08%3A_Ferro-_Ferri-_and_Antiferromagnetism

Orbital Compensation

Arrows are magnetic moments of each sublattice, iron in white and rare-earth in orange

Rare-earth moment responds more strongly to T near T_c

$\mu \propto L$ and S

At T_c, μ drops to 0

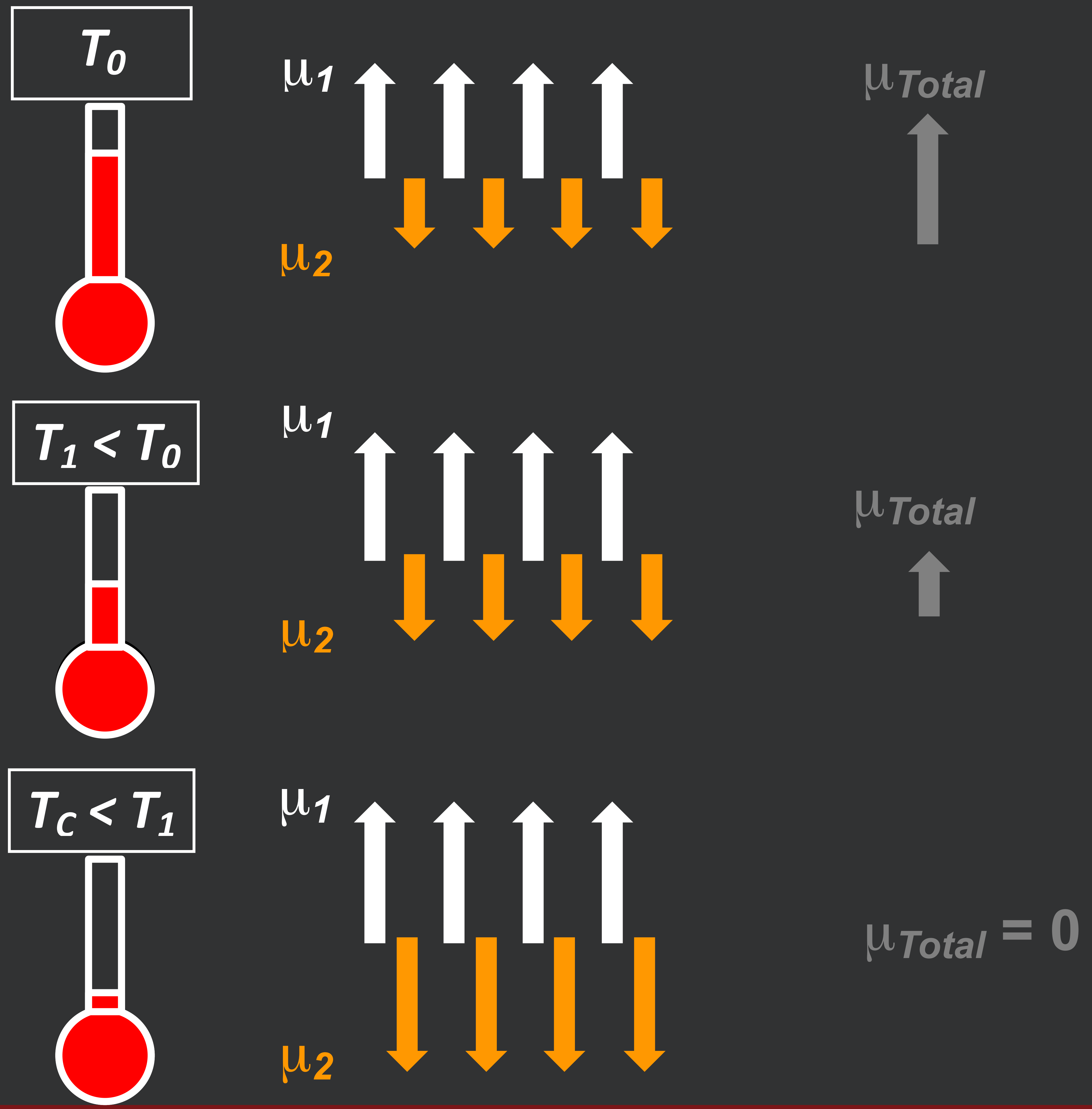

Orbital Compensation

Arrows are magnetic moments of each sublattice, iron in white and rare-earth in orange

Rare-earth moment responds more strongly to T near T_c

$\mu \propto L$ and S

At T_c, μ drops to 0 but net spin non-zero due to L:

$\mu_{Fe} \propto S$ only

$\mu_{Tb} \propto S$ **and** L

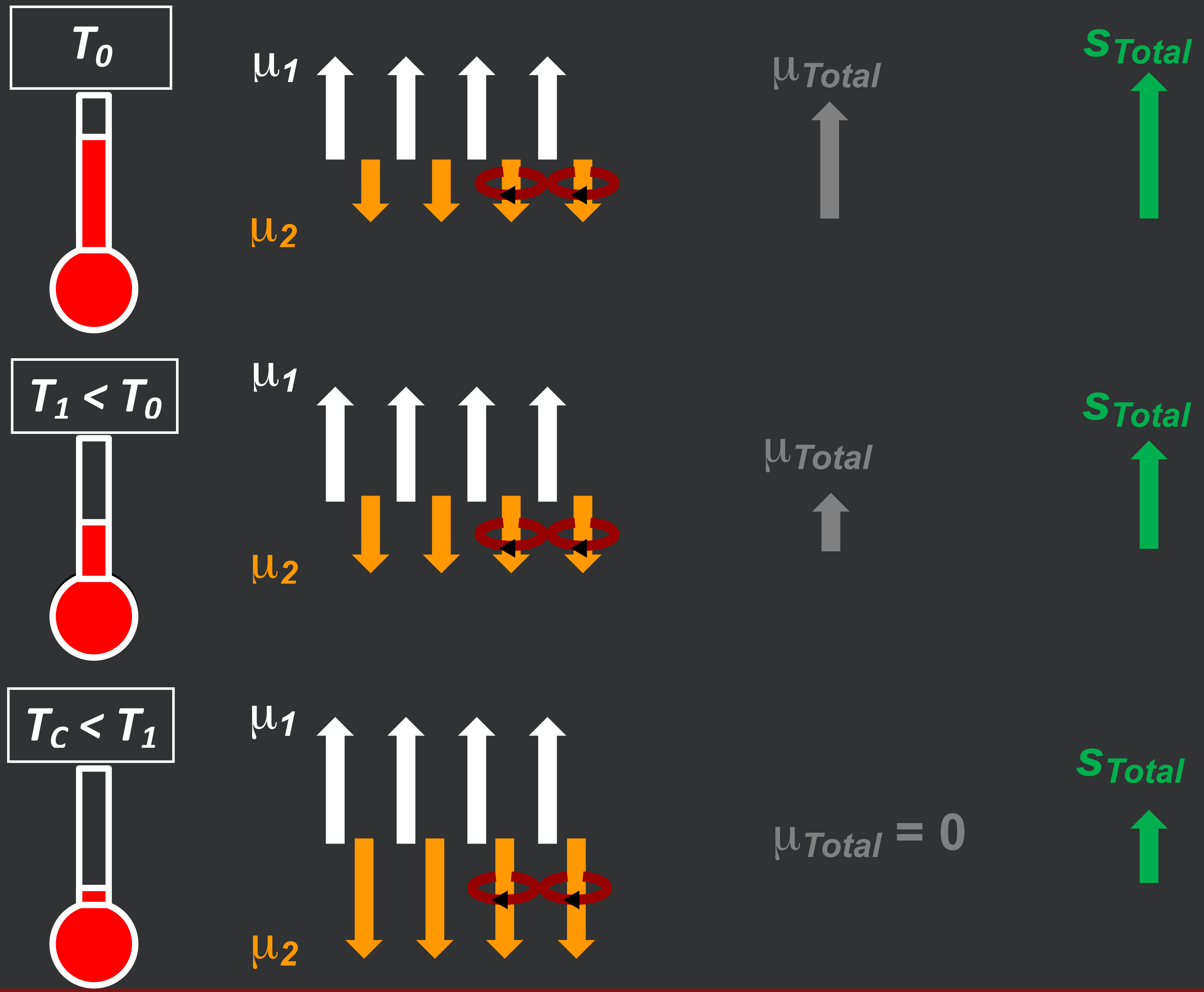

Rare-Earth Iron Garnets (*R*IG)

Ferrimagnets of the form $R_3Fe_5O_{12}$ where R is Dy, **Tb**, Gd, Yb, Ho, Er

Garnet refers to the crystal structure

Temperature-dependent orbital compensation of magnetism associated with spin

T_{comp} below room temperature, but accessible with LN or ethylene glycol

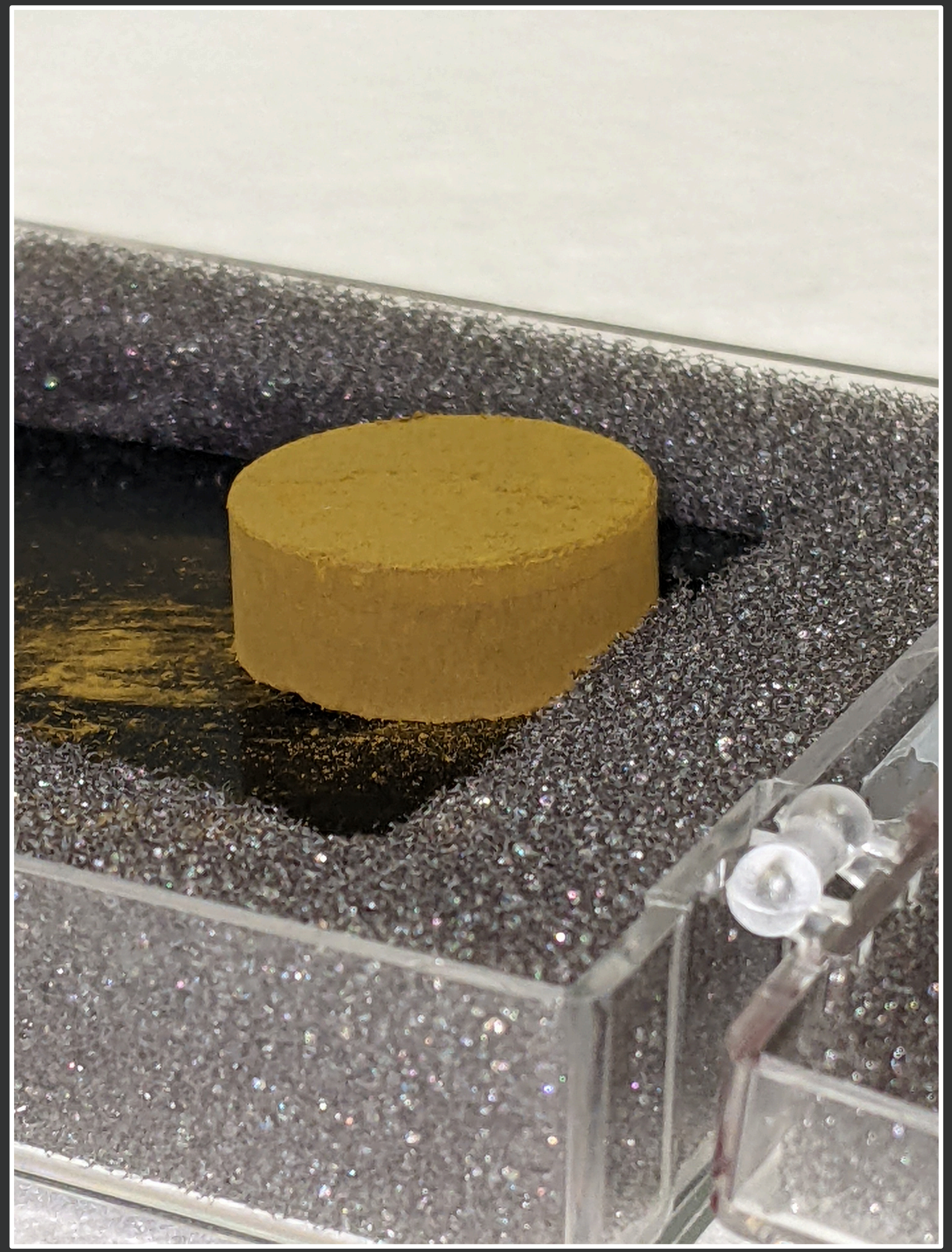

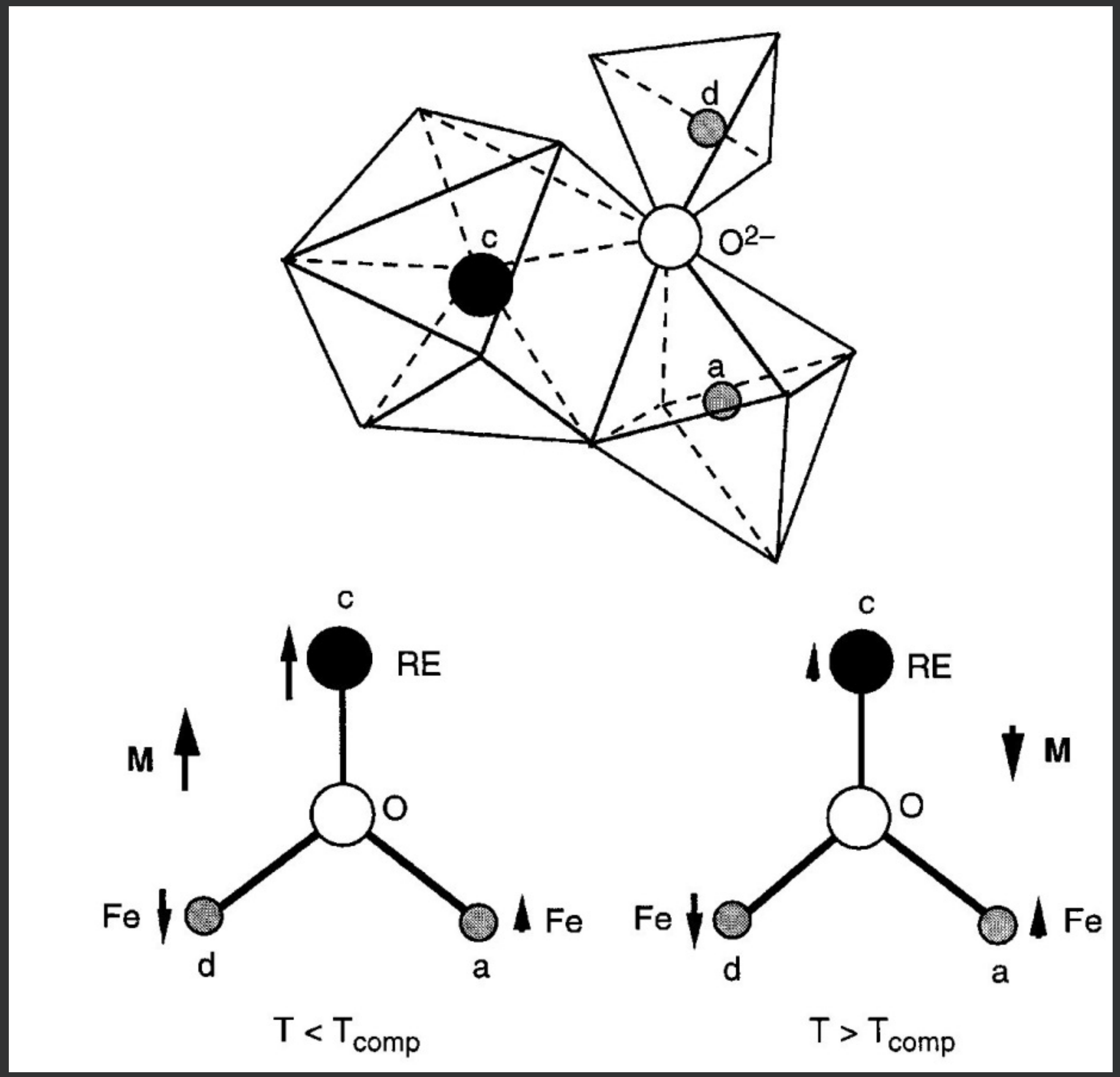

G. Dionne, *Magnetic Oxides* (N.Y., Springer, 2009)

Why Terbium?

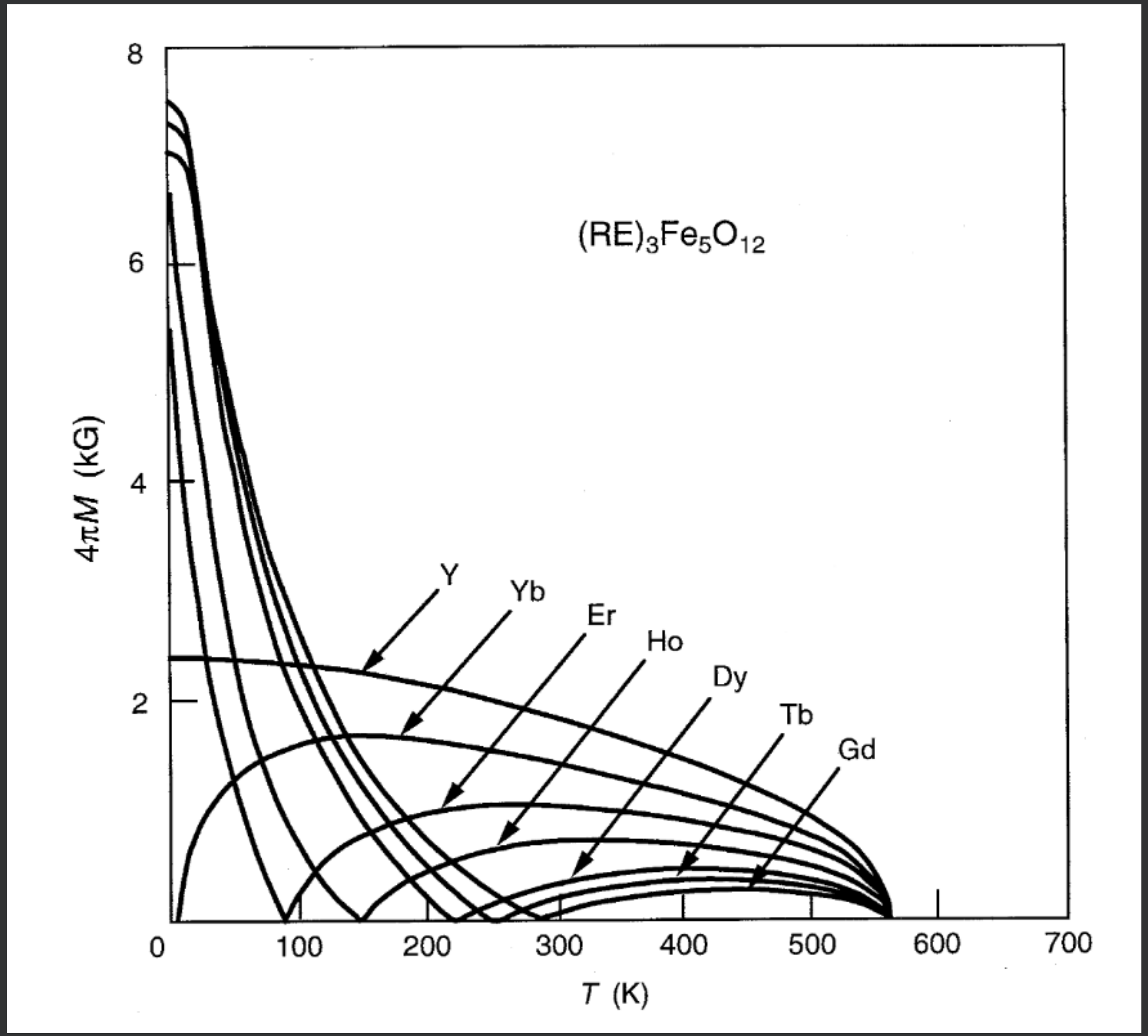

G. Dionne, *Magnetic Oxides* (N.Y., Springer, 2009)

Easily accessible T_{comp} (~250 K) with modest cooling schemes (LN or ethylene glycol)

TbIG has low neutron absorption — this allows for a thicker target and more precision in n spin rotation measurement

Novel source of polarized electron spin

TbIG Neutron Measurements Timeline

2020

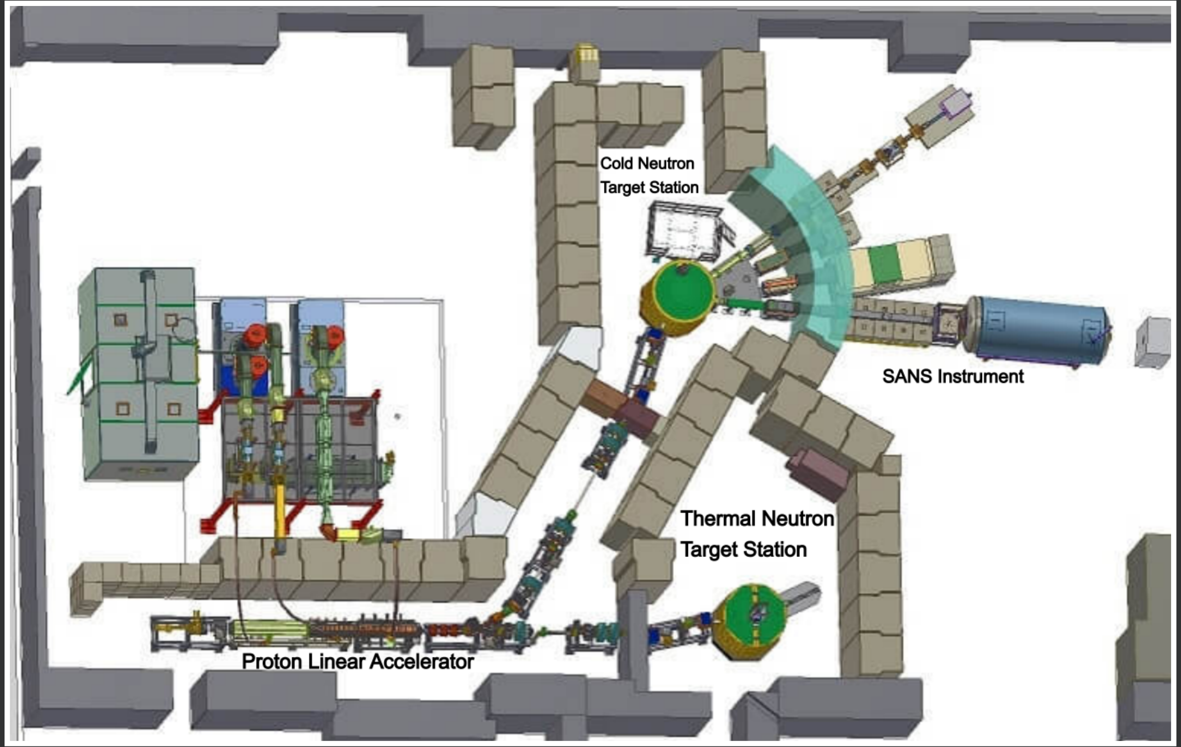

IU LENS

Jan. 2023

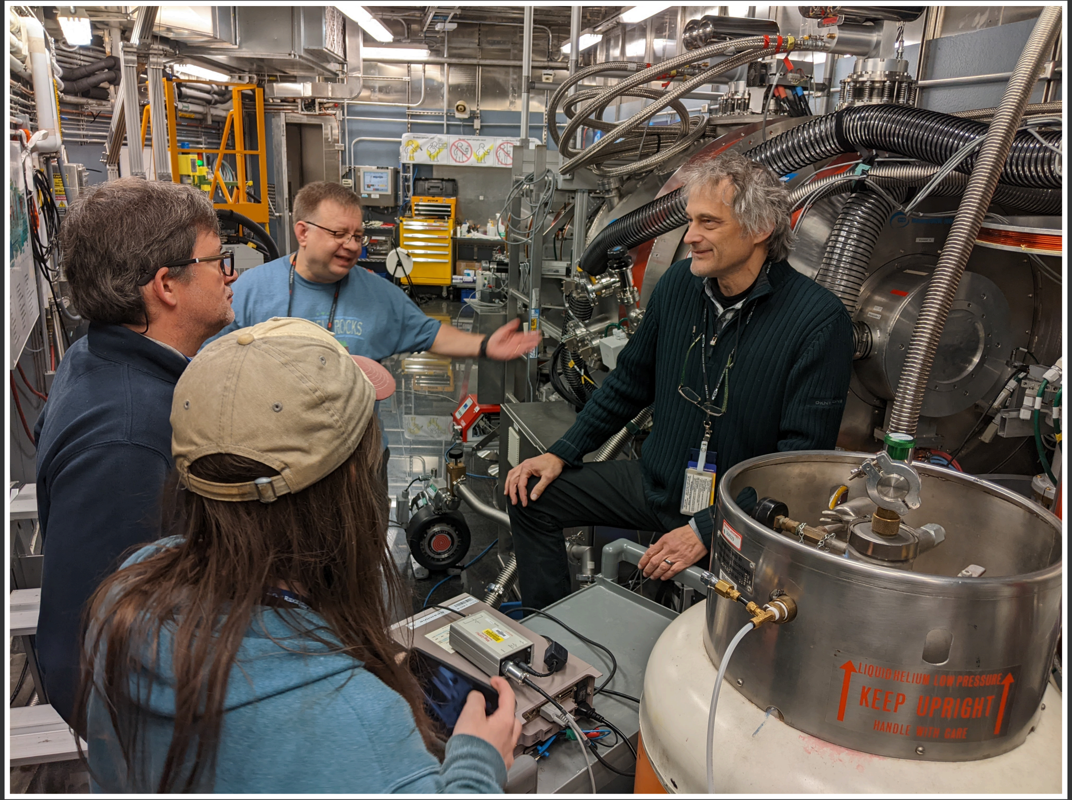

SNS-NSE (BL-15)

July 2023

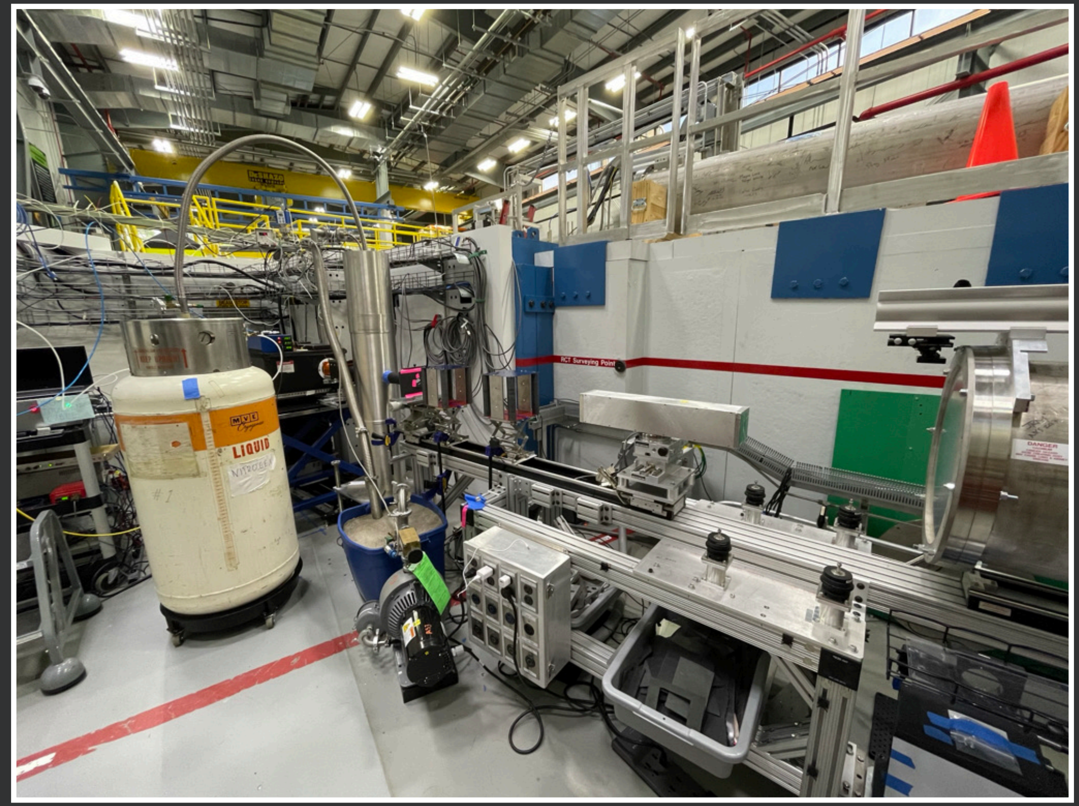

HFIR-MARS (CG-1D)

June 2024

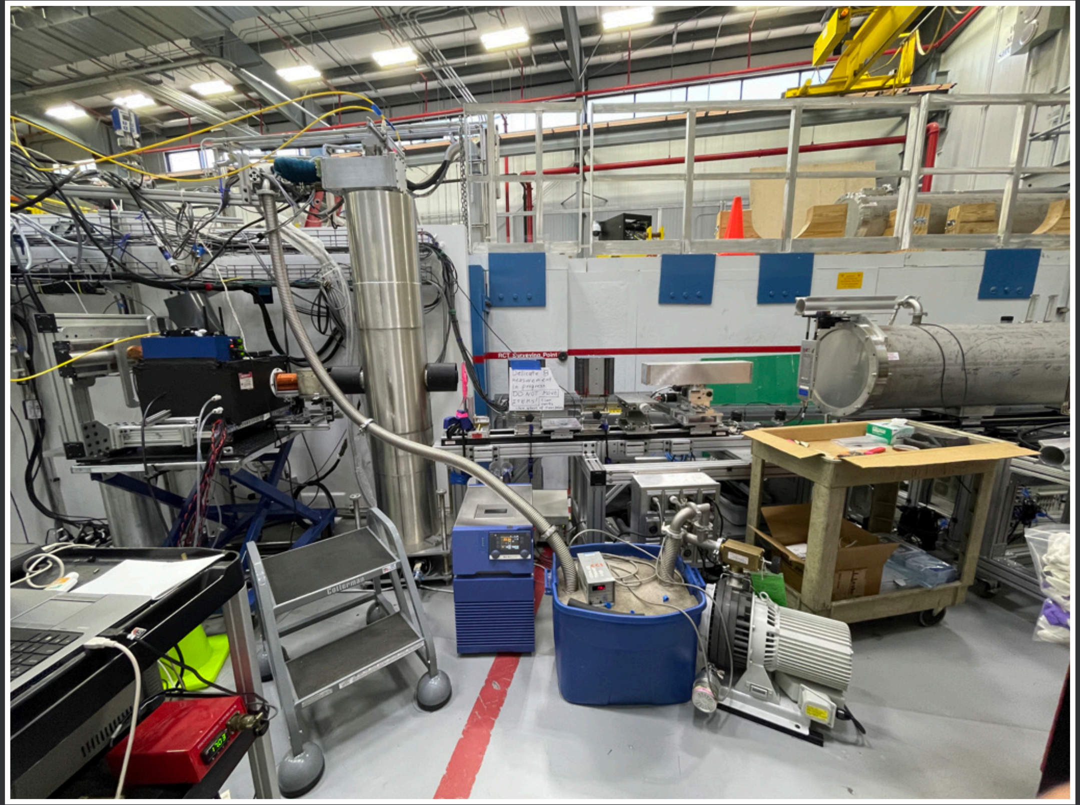

HFIR-MARS (CG-1D)

MARS

Multimodal Advanced Radiography Station (MARS)

HFIR beamline CG-1D

Radiography and computed tomography imaging capabilities

High spatial resolution radiography to quantify n-spin rotation

Neutron Flight Path

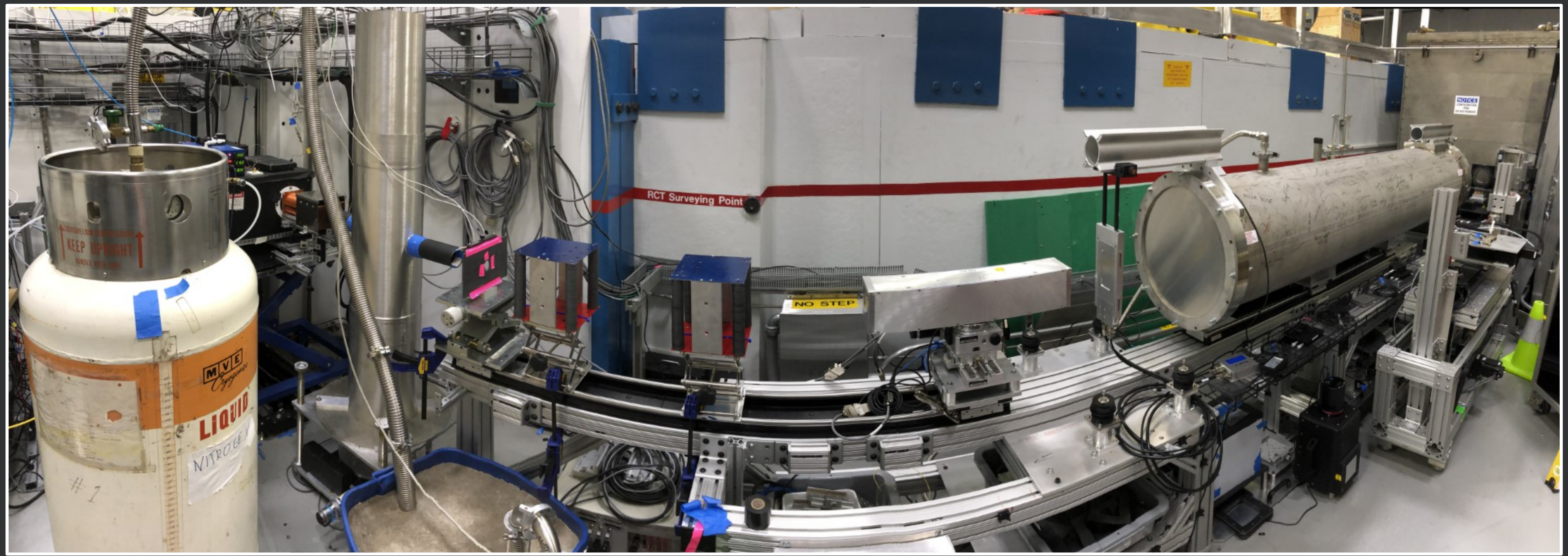

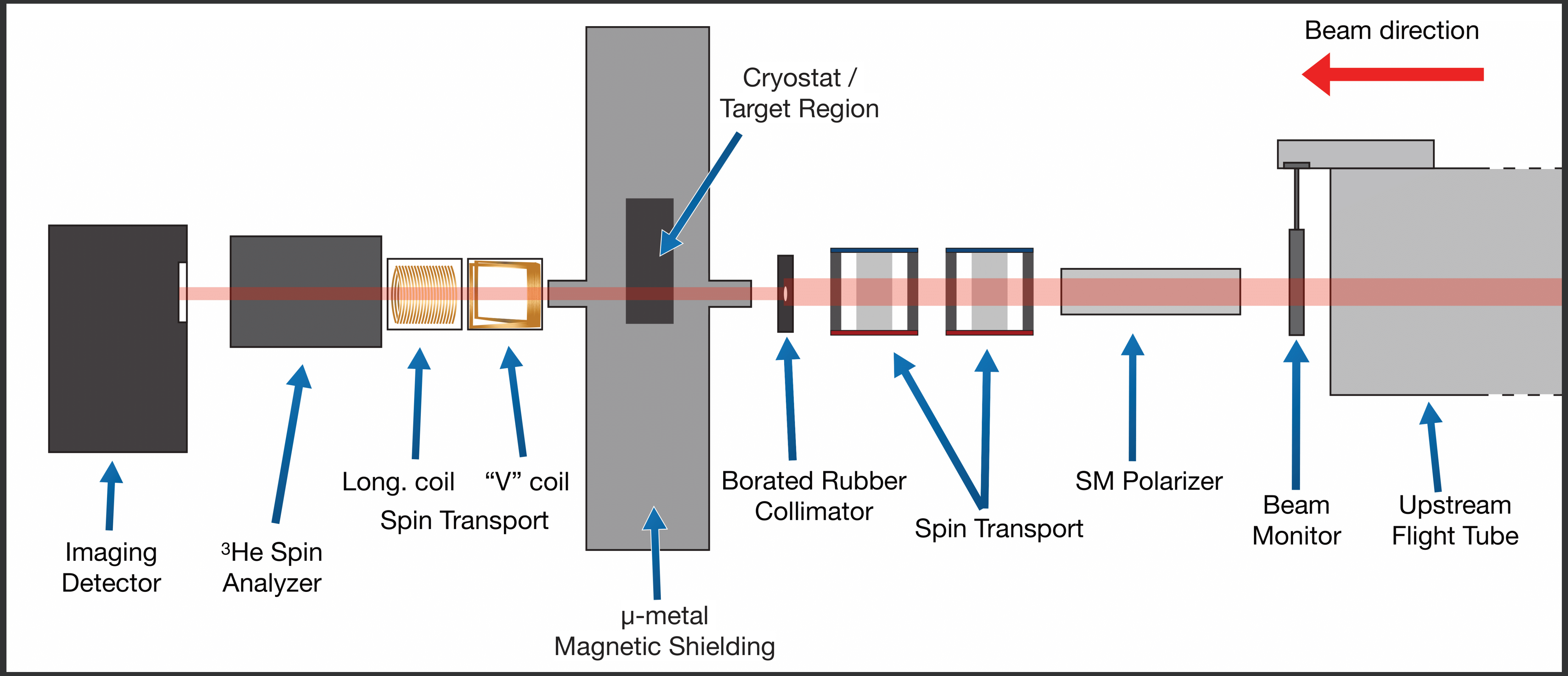

Flight Tube / Beam Monitor

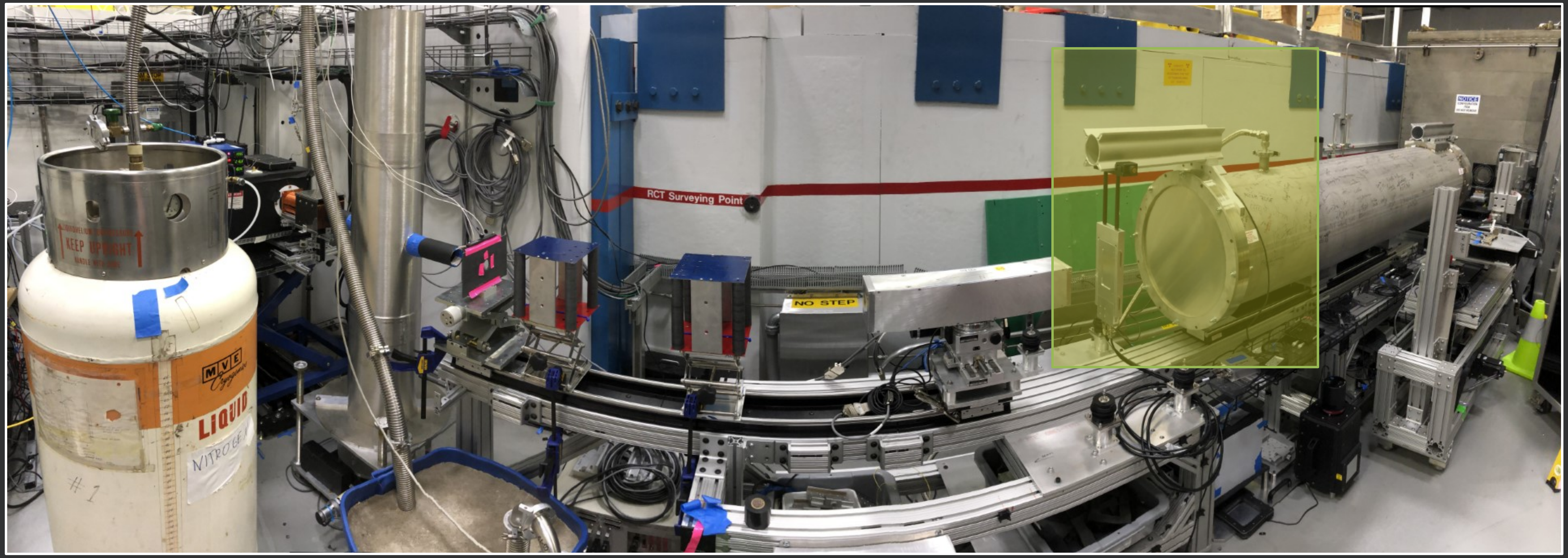

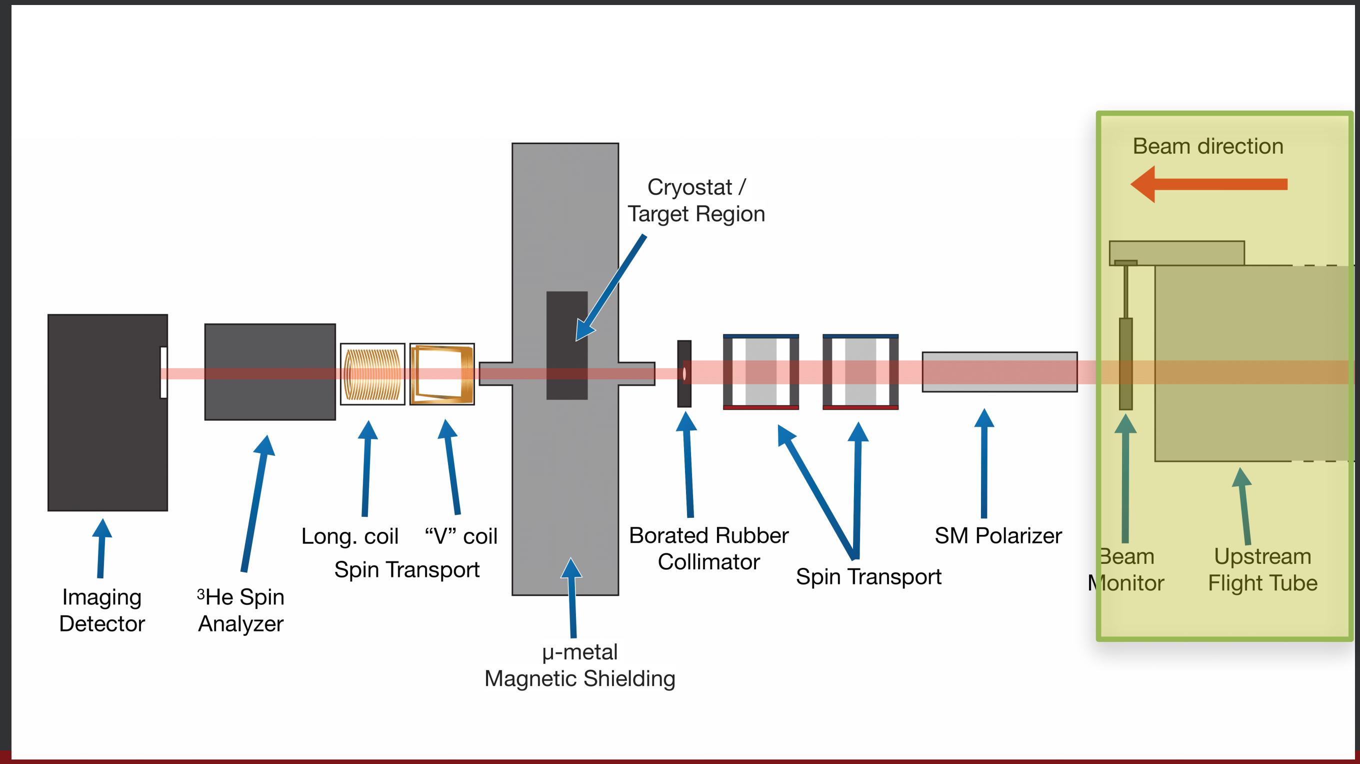

Polarizer

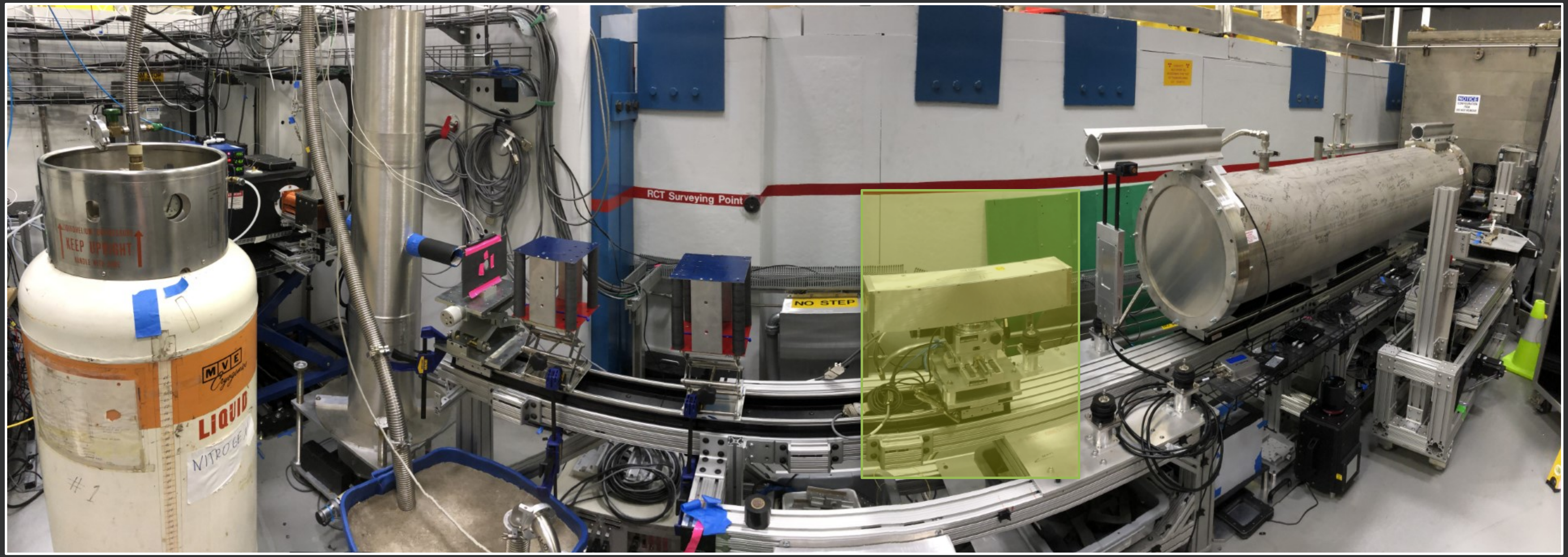

Swiss Neutronics V-cavity supermirror polarizer

Uses magnetic layers and an externally applied B-field:
—> spin-aligned neutrons are reflected while spin anti-aligned neutrons are transmitted into absorbing substrate

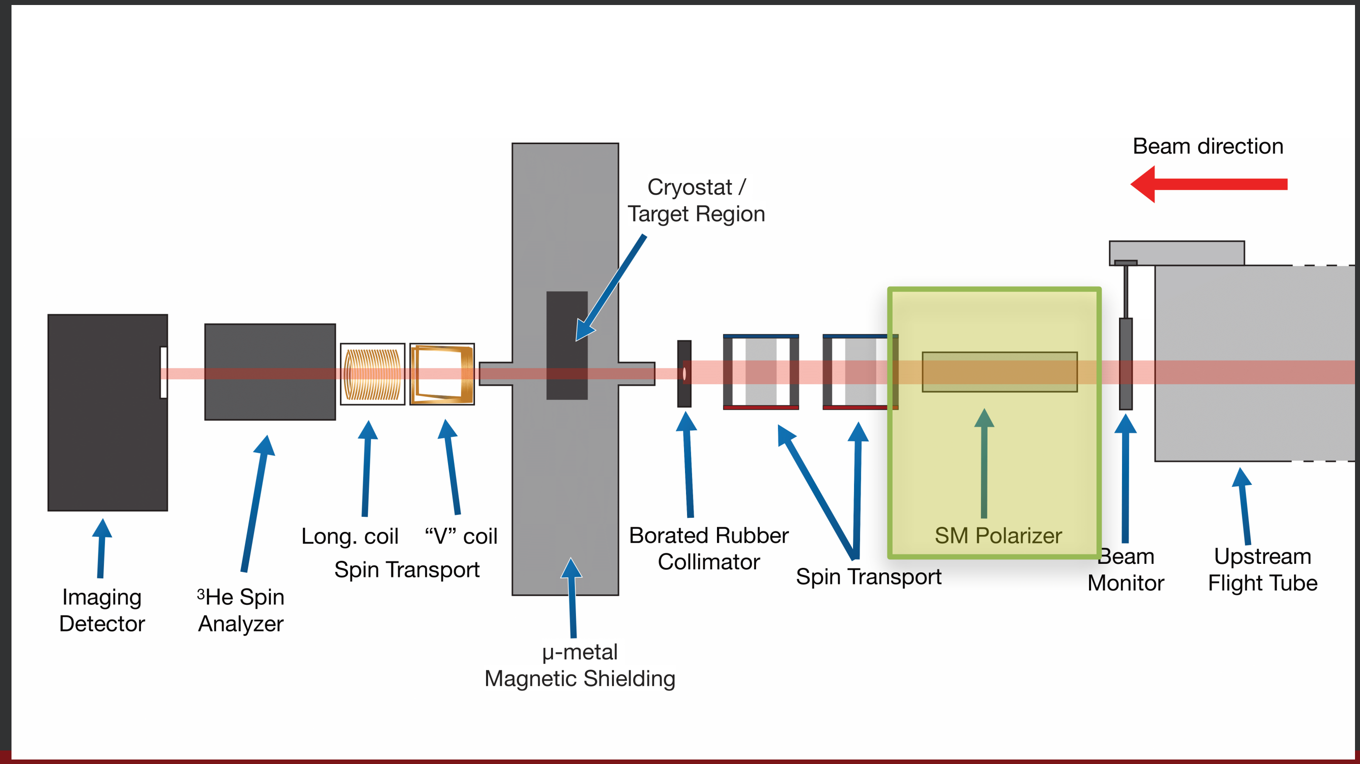

Spin Transport

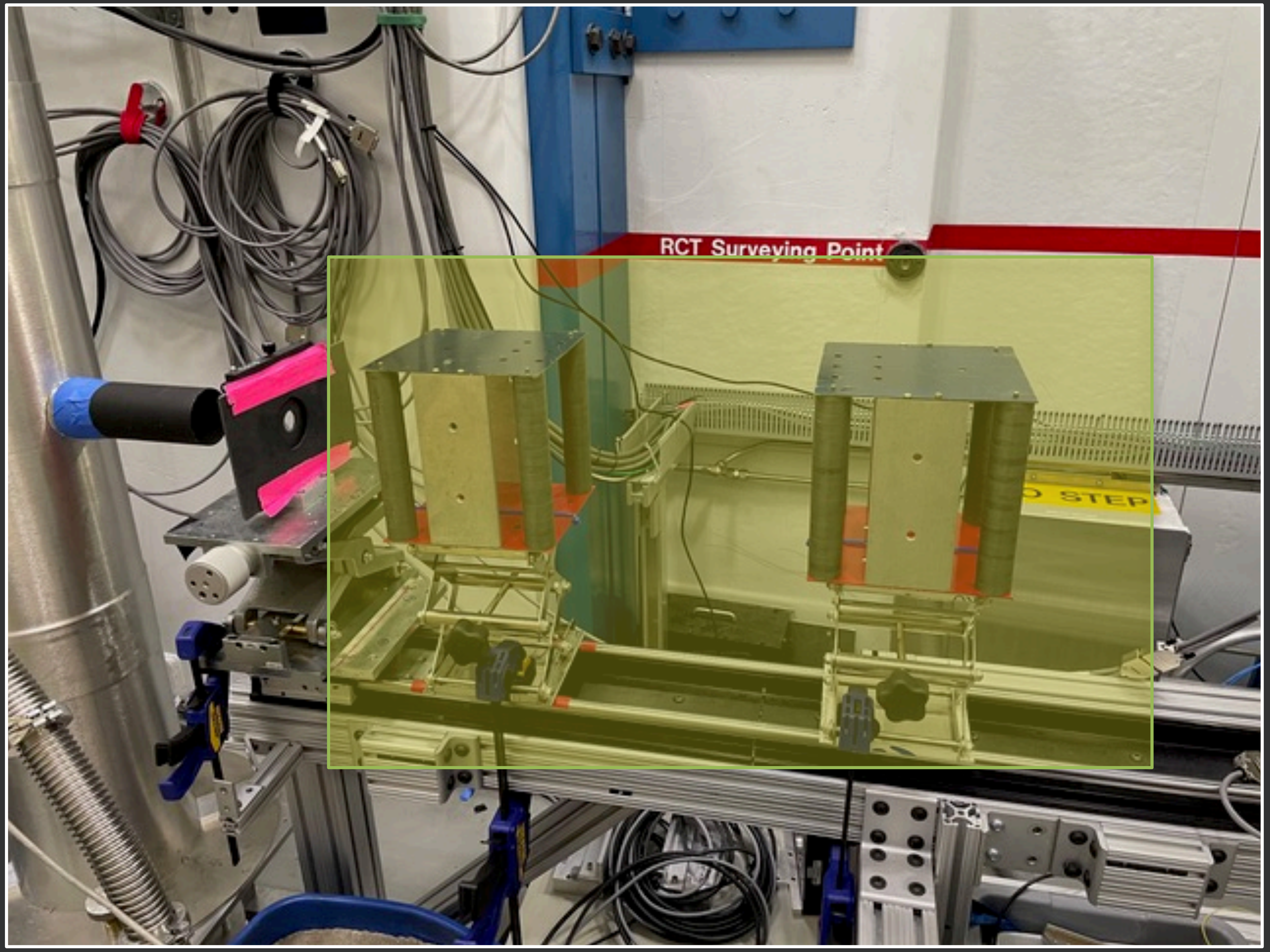

Guide field elements maintain polarization along n travel

> 90 Gauss at center

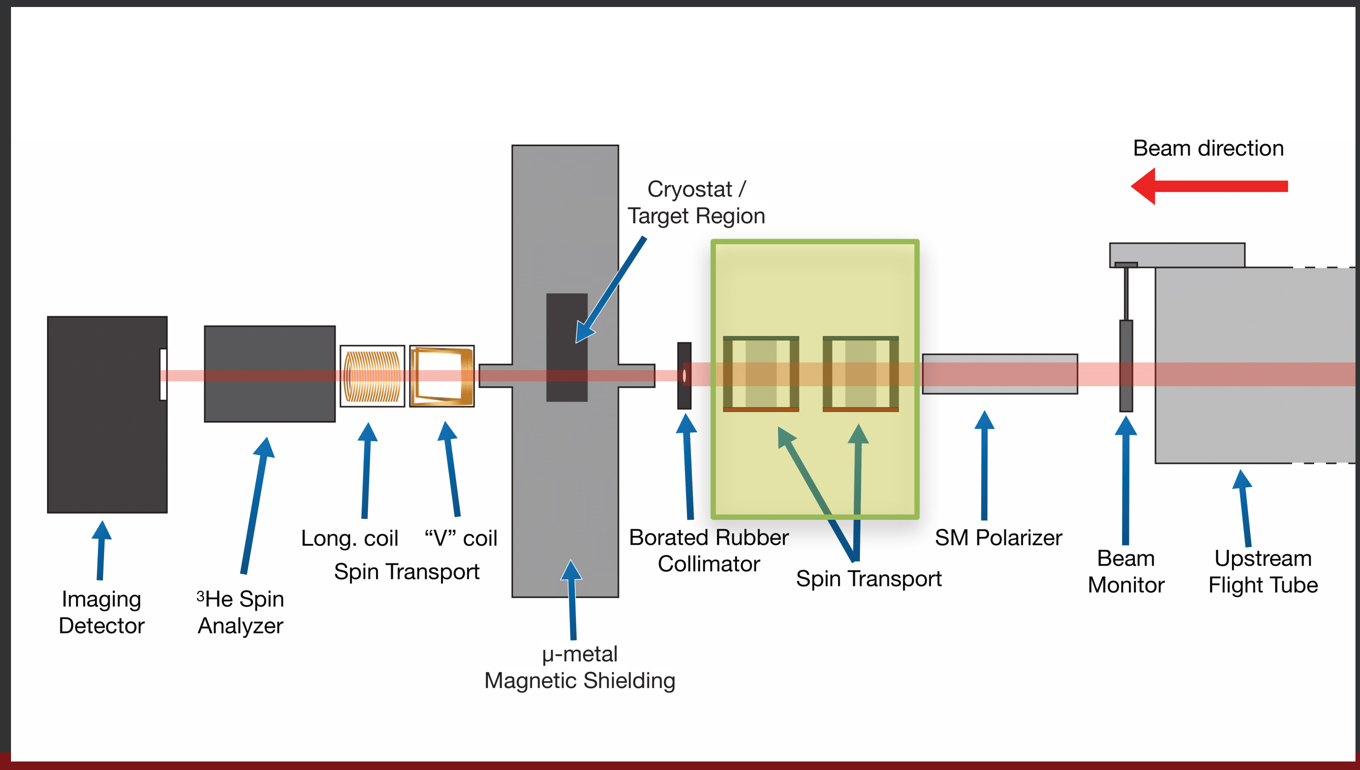

Spin Manipulation

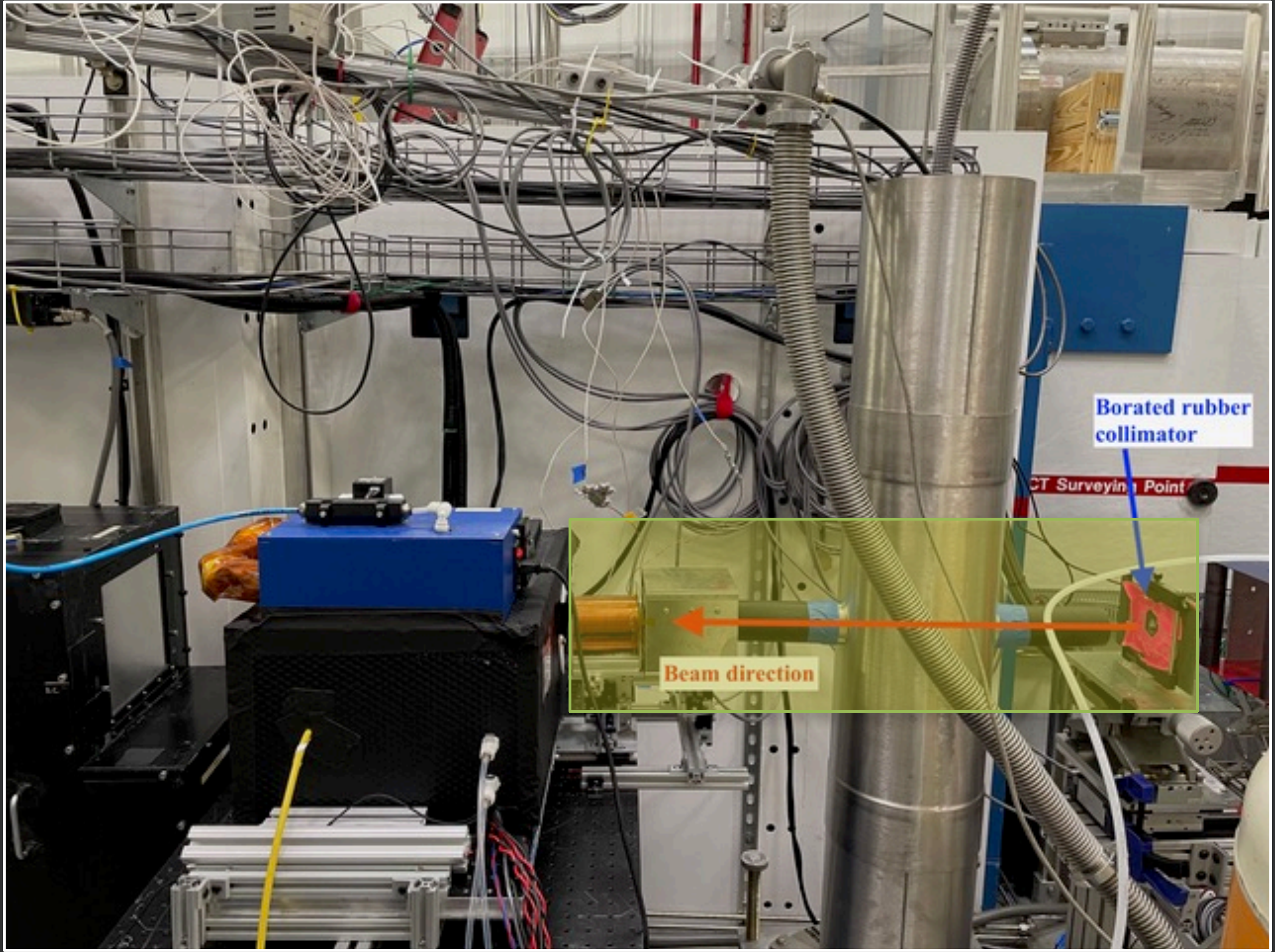

Beam collimated

Neutrons pass through sample and spin rotate

Exit to V-Coil (Forte Coil)
- Diabatic transition via current sheet

Exit to longitudinal coil
- Adiabatic rotation

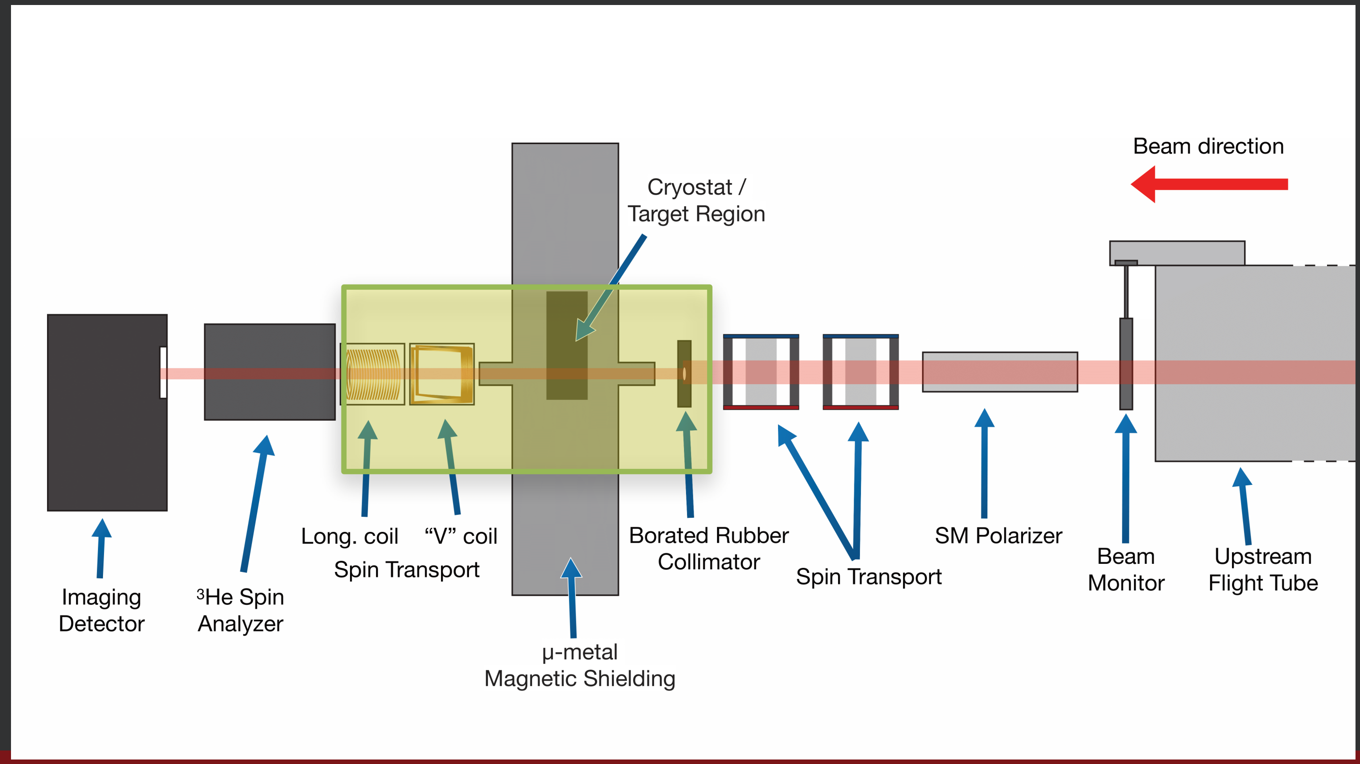

Spin Analyzer

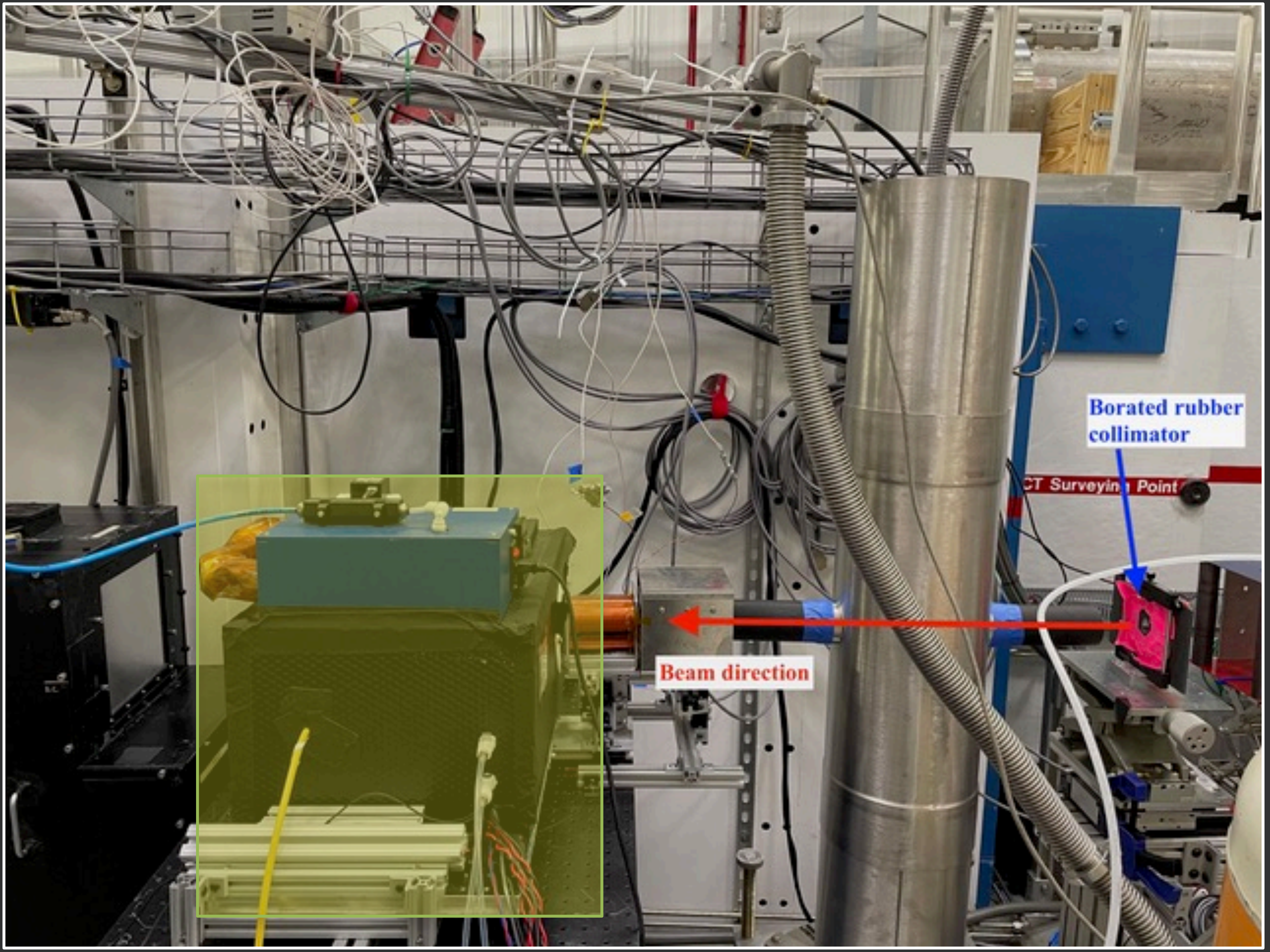

^{3}He neutron spin analyzer (courtesy of Chenyang Peter Jiang)

Longitudinal polarization direction (aligned to beam momentum)

~0.84 calculated analyzer efficiency

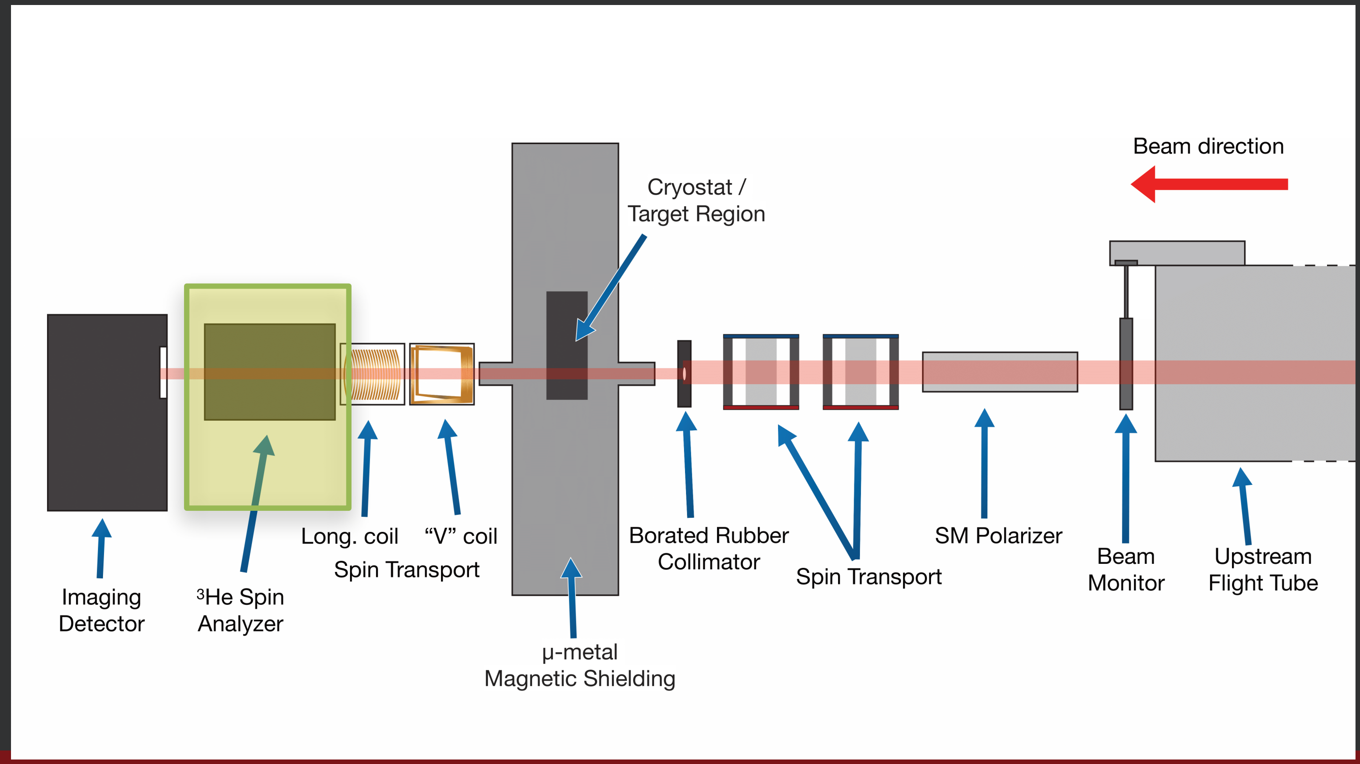

Neutron Imaging Detector

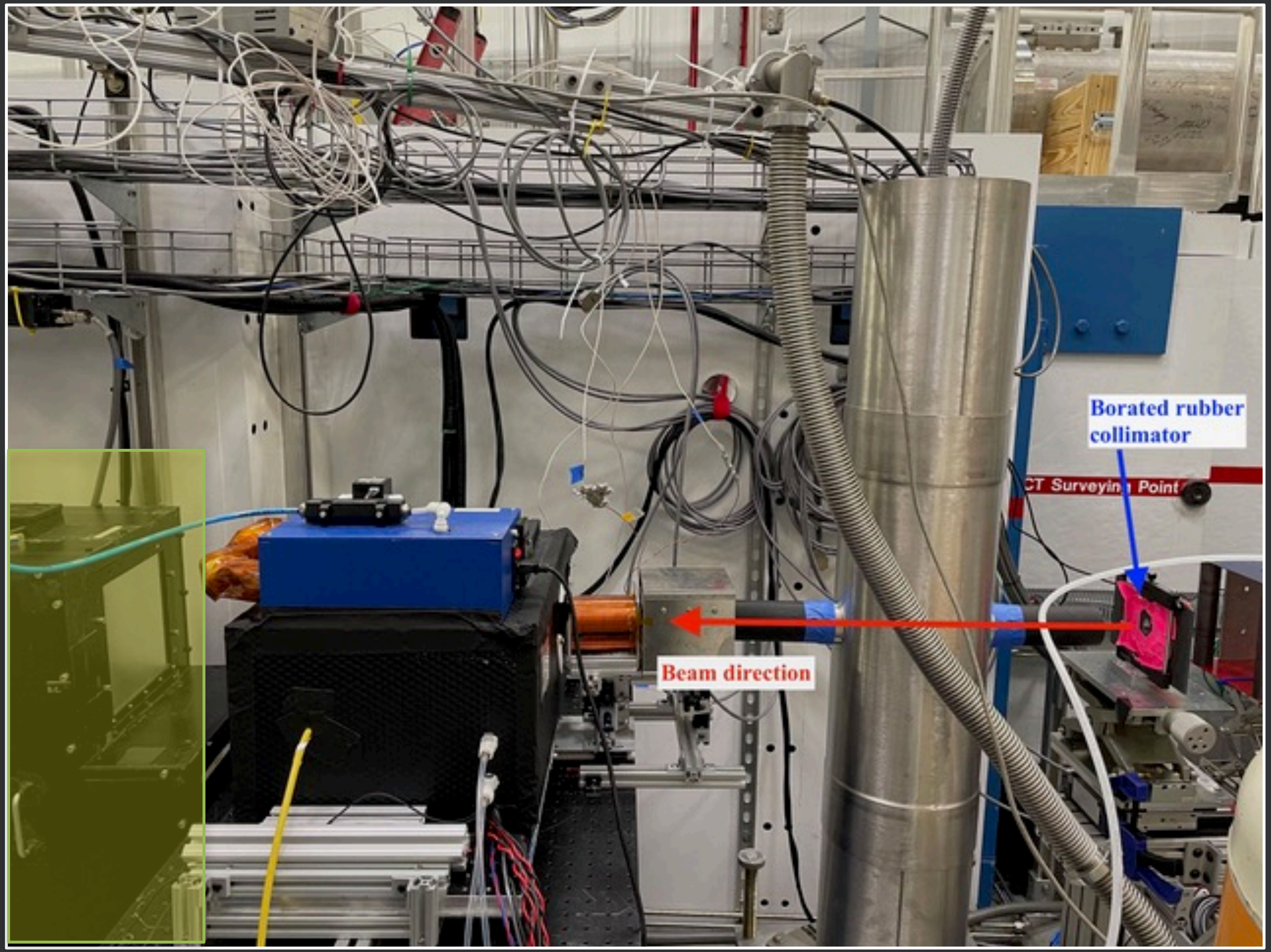

CCD imaging detector

^{6}LiF/ZnS:Cu scintillator

2048x2048 pixels, 42 μm pixel size

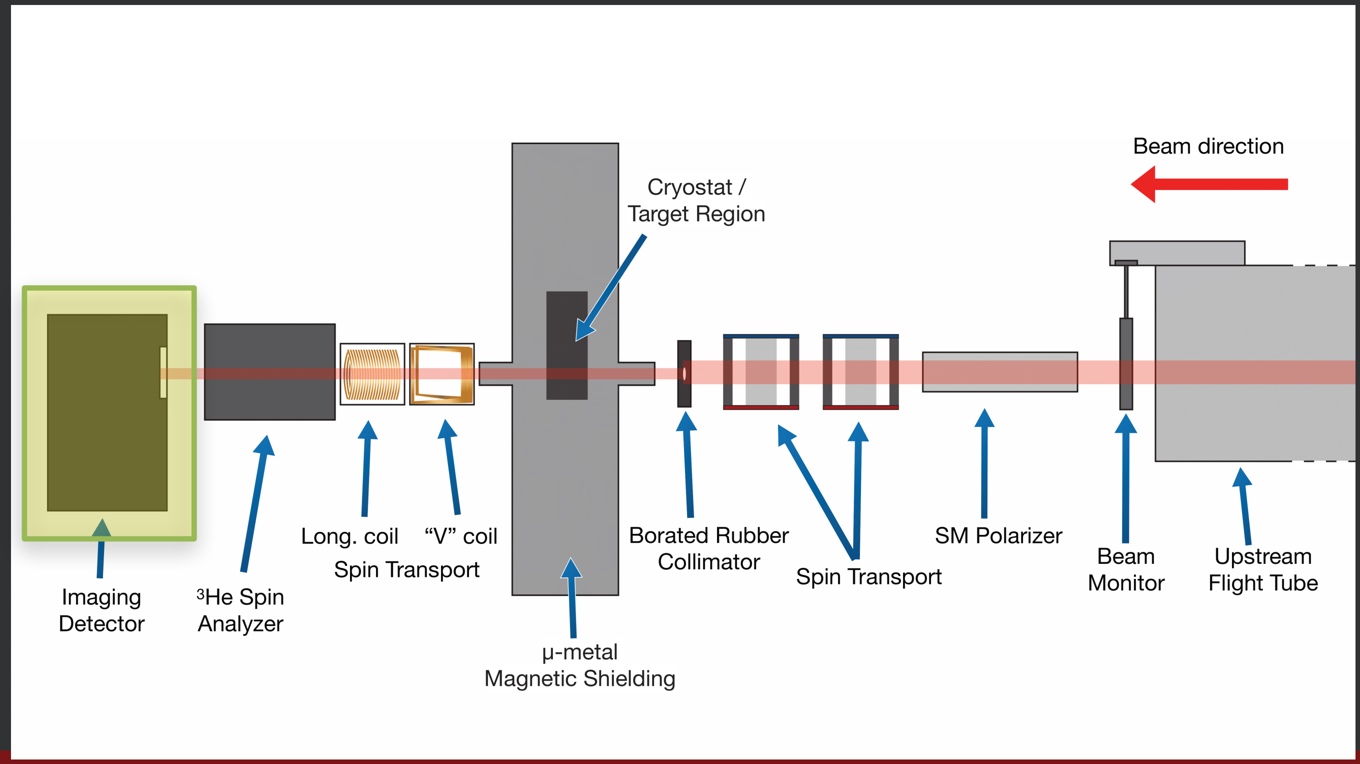

MARS 2023

Target Region

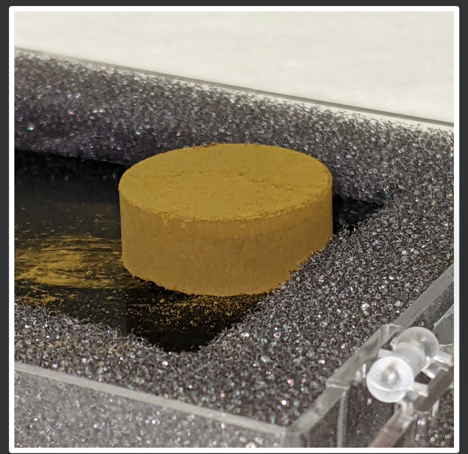

Sample

Inside of Cryostat

Cryostat

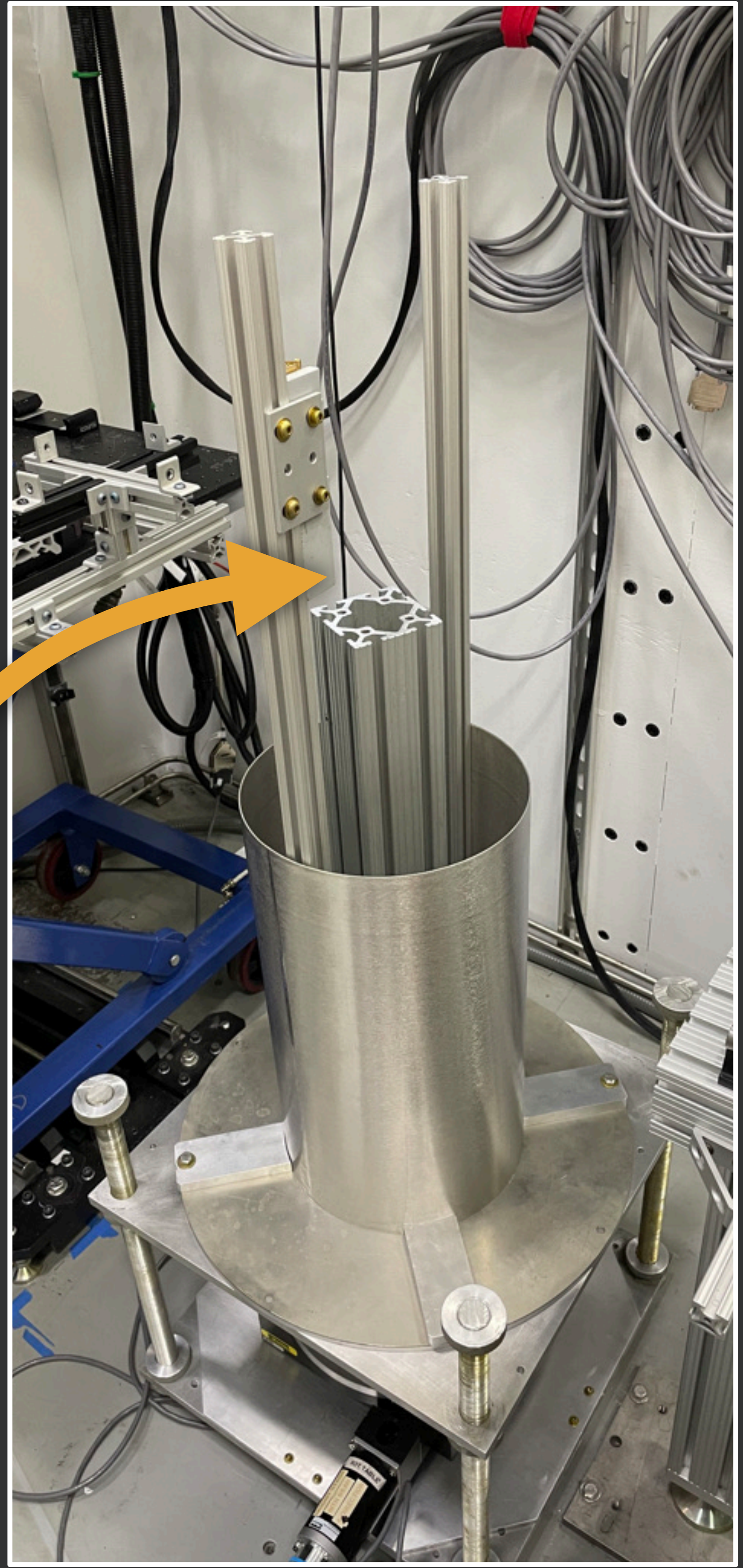

80/20 support

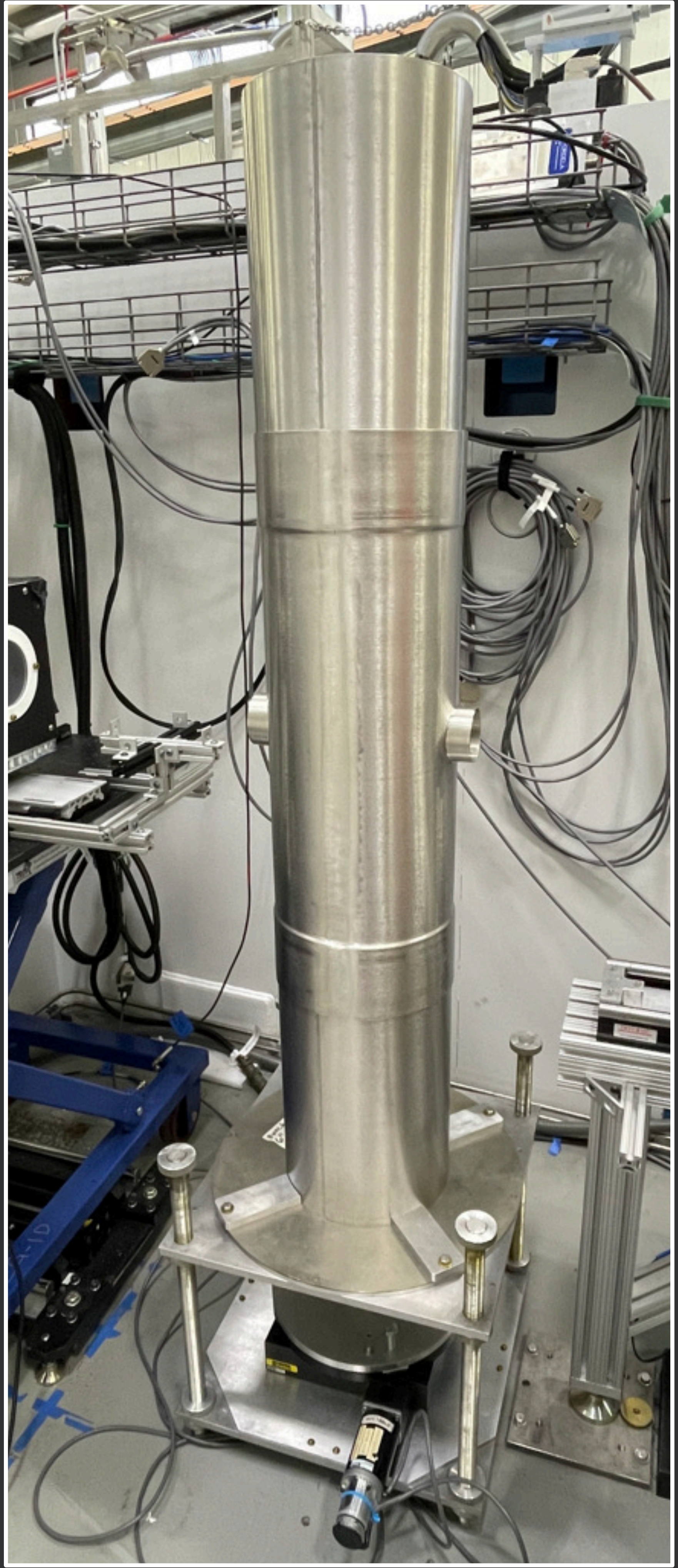

Mu-metal Shielding

Neutron Spin Orientation

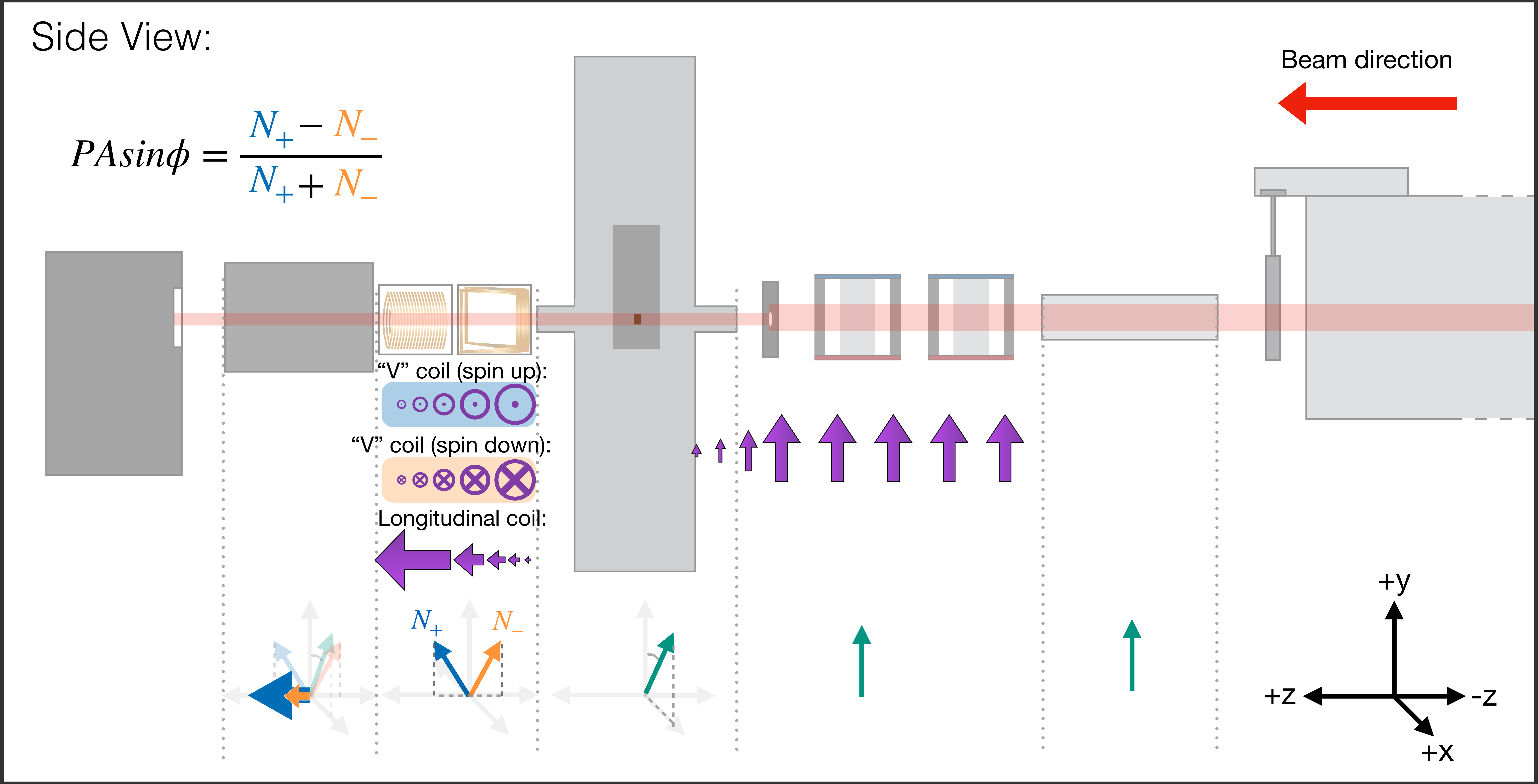

Measurement Strategy

Asymmetry measurement: spin-up vs. spin-down via V-coil current flips

DATA SETS:
1. Ferrimagnetics checked (temp sweep through T_c)

2. Fifth-force @ T_c with 180° rotation

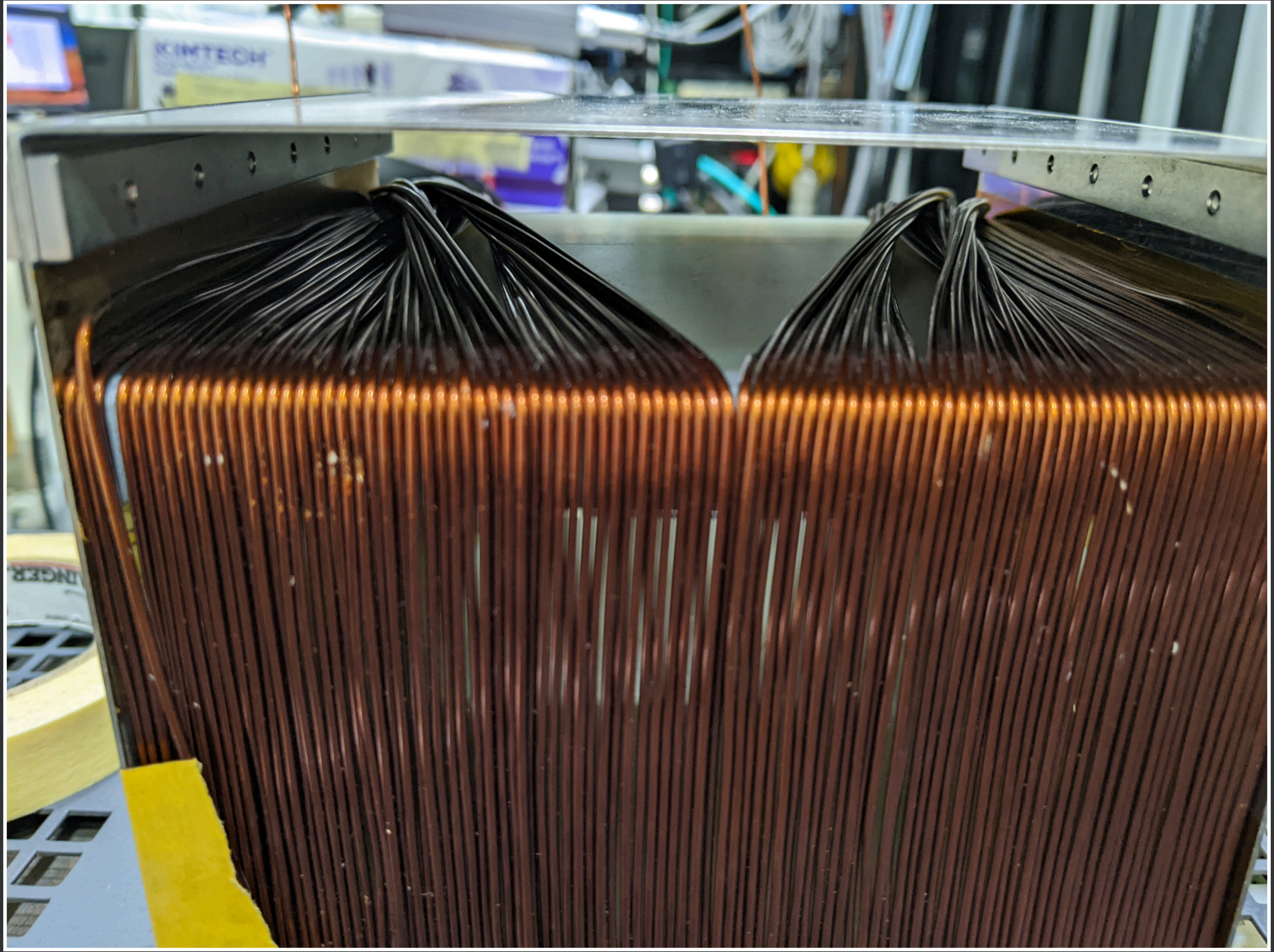

Image of V-coil current sheet (neutron view)

Temperature Sweep Data

Pixel brightness ∝ neutron count

Brighter —> spin rotated into analyzation direction

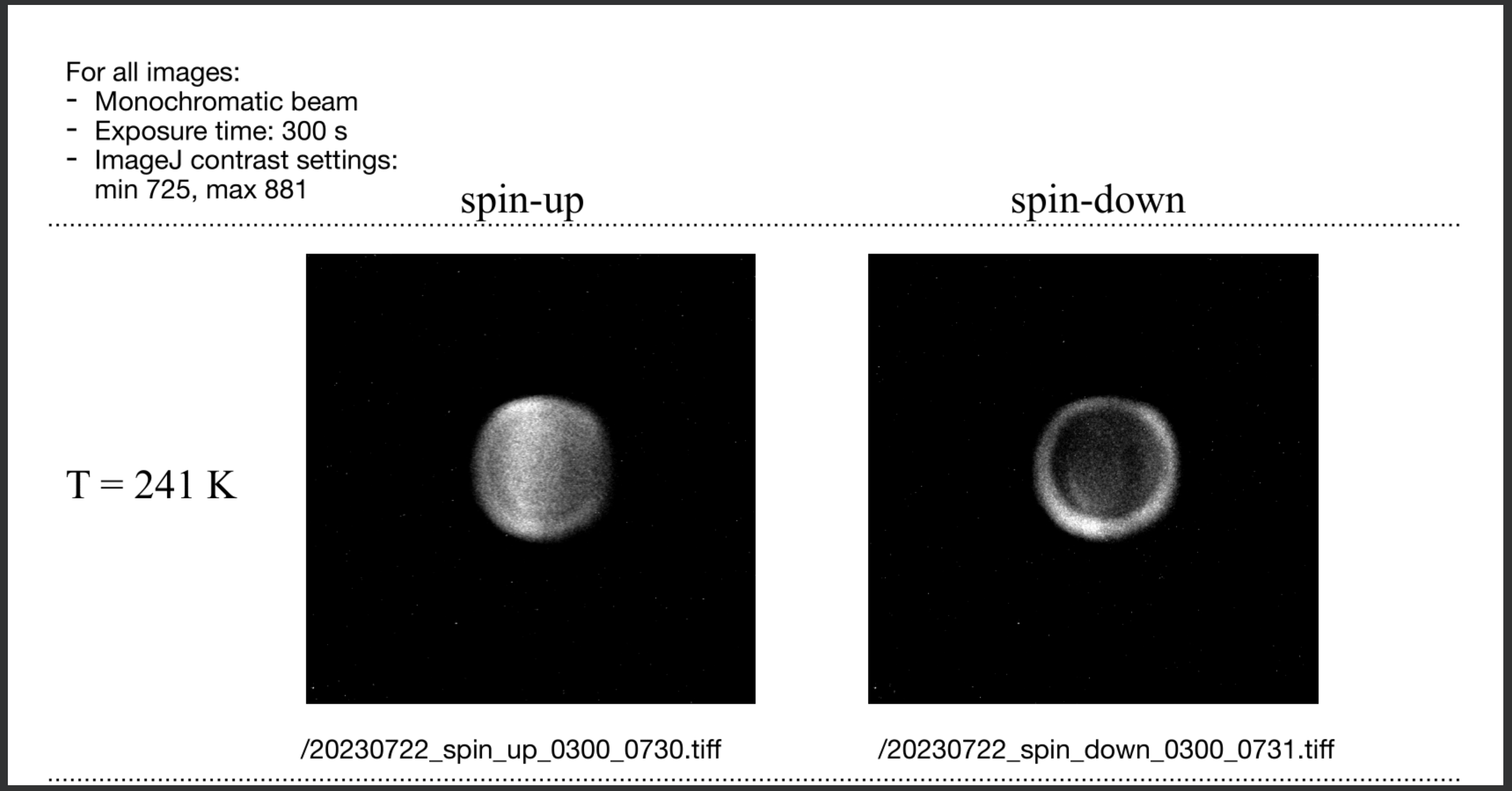

Temperature Sweep Data

Pixel brightness ∝ neutron count

Brighter —> spin rotated into analyzation direction

Equal intensity —> no difference

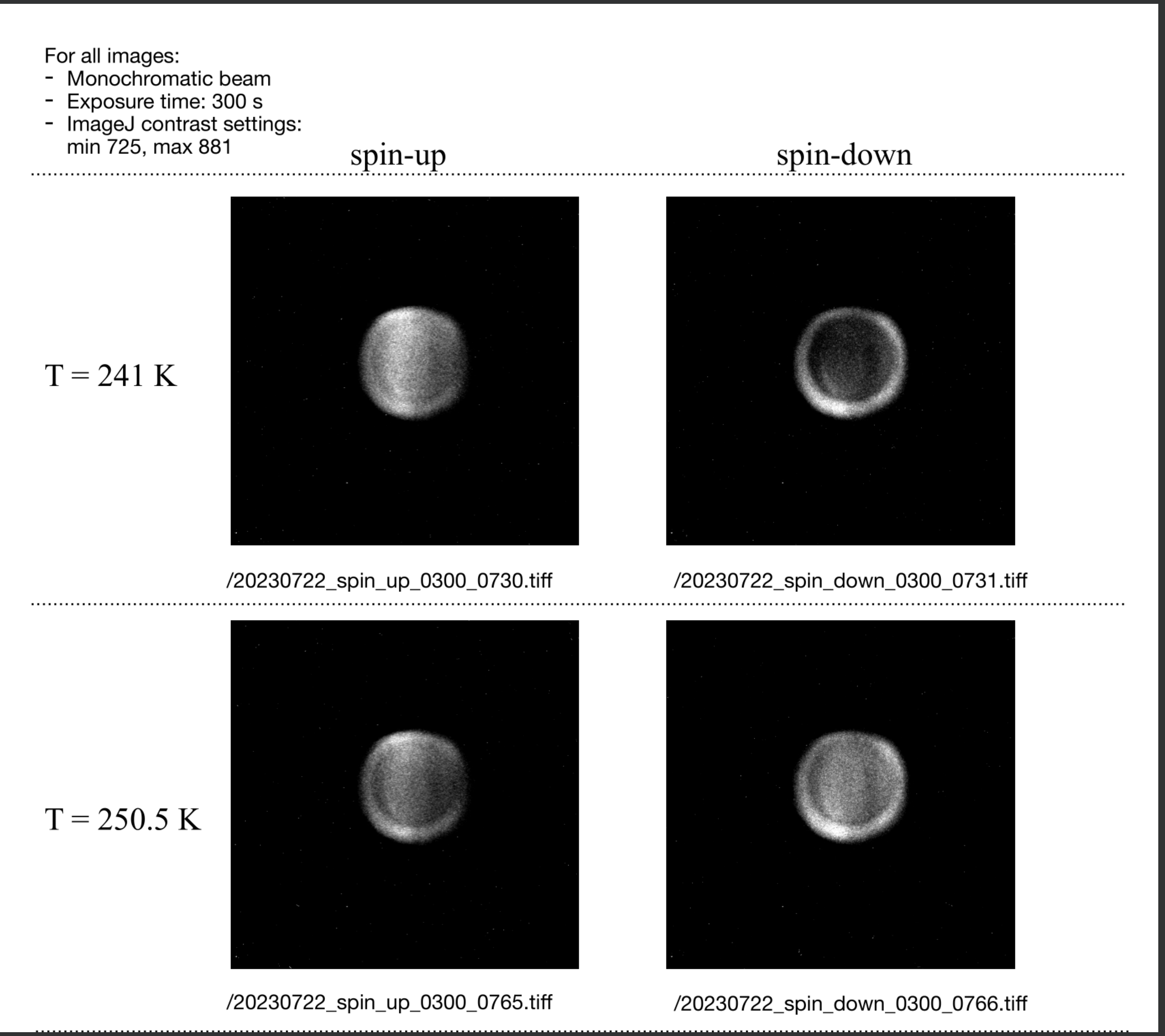

Temperature Sweep Data

Pixel brightness ∝ neutron count

Brighter —> spin rotated into analyzation direction

Equal intensity —> no difference

Reversal of signal through T_c

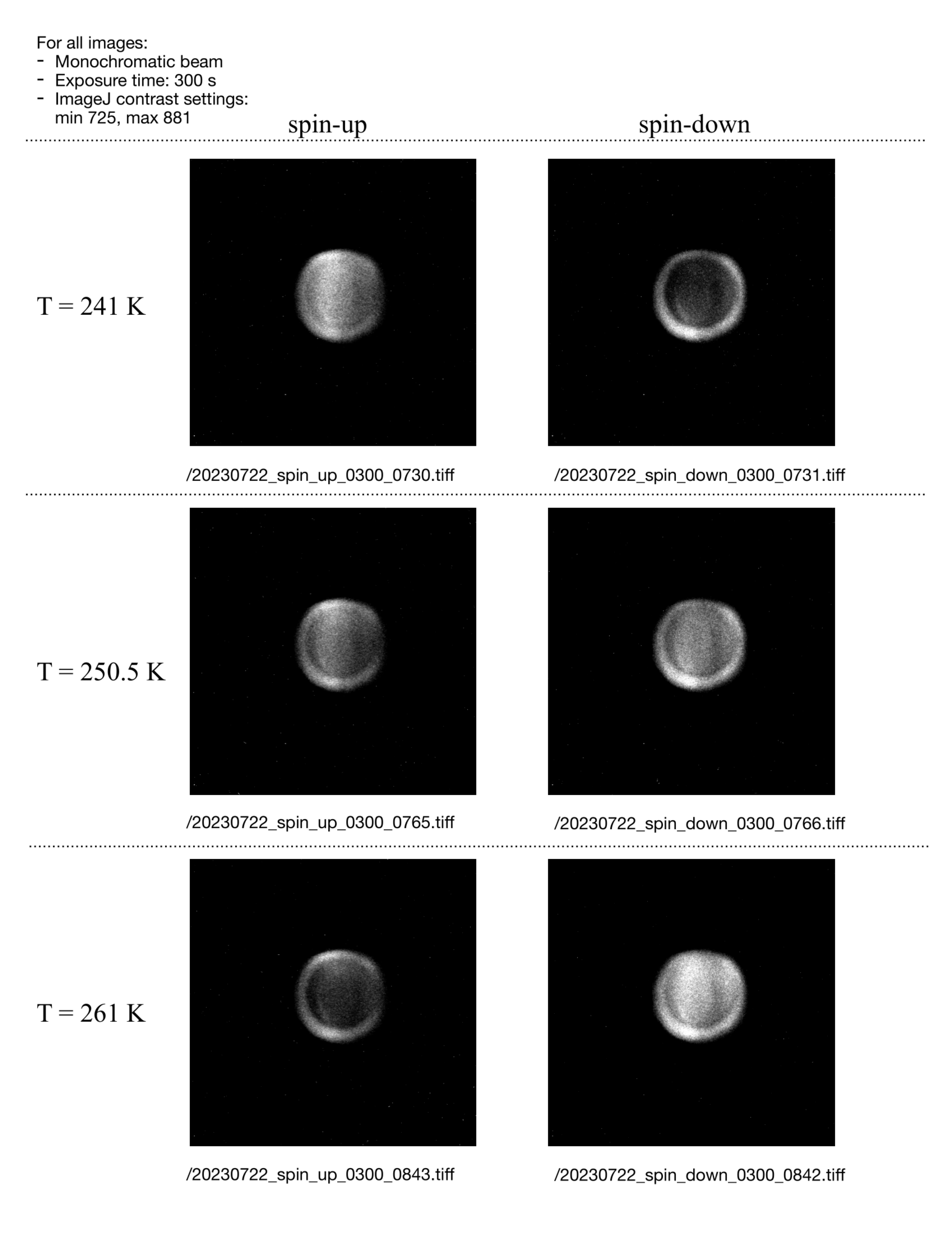

Fifth-Force Data

Asymmetry value:
$\left(-1.99 \pm 9.62\right) \times 10^{-5}$

Asymmetry involves both N_+ and N_- neutron spin rotation states as well as 0° and 180° target rotation states

Consistent with 0

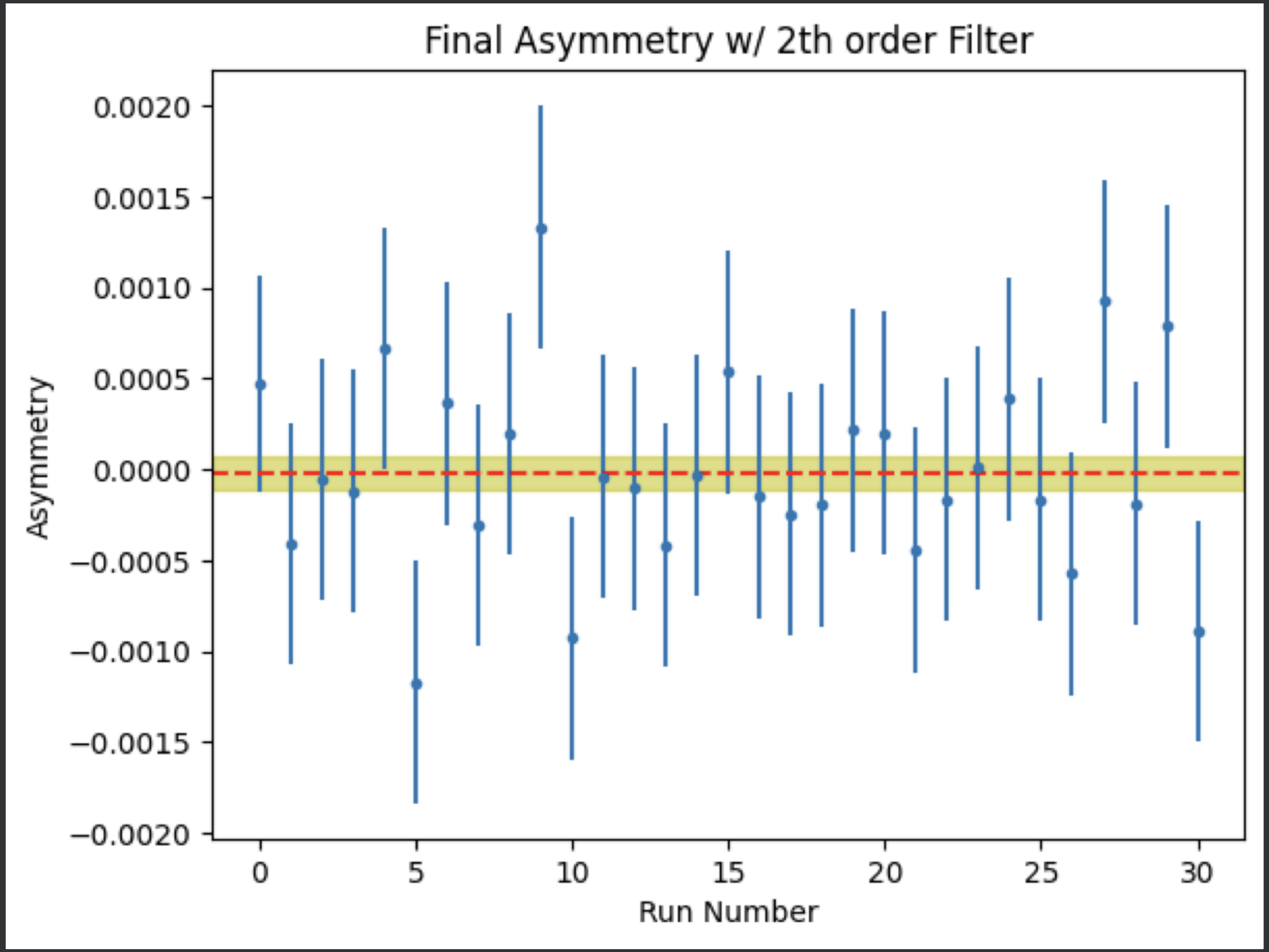

MARS 2024


RCT Surveying Point
Delicate B measurement in progress
DO NOT move items!

Improvements

Cryostat modification
- all non-mag materials
- “coffin” sample case, better thermal contact
- improved magnetometry, thermometry
- ethylene glycol cooling
- improvement of rotation mechanism

Second layer of mu-metal shielding
- ~100x shielding factor

Upgraded imaging detector
- previously: CCD, ^{6}LiF/ZnS:Cu scintillator, 2048x2048 with 42 μm pixel size
- new: CMOS, GadOx scintillator, 6200x6200 with 16 μm pixel size

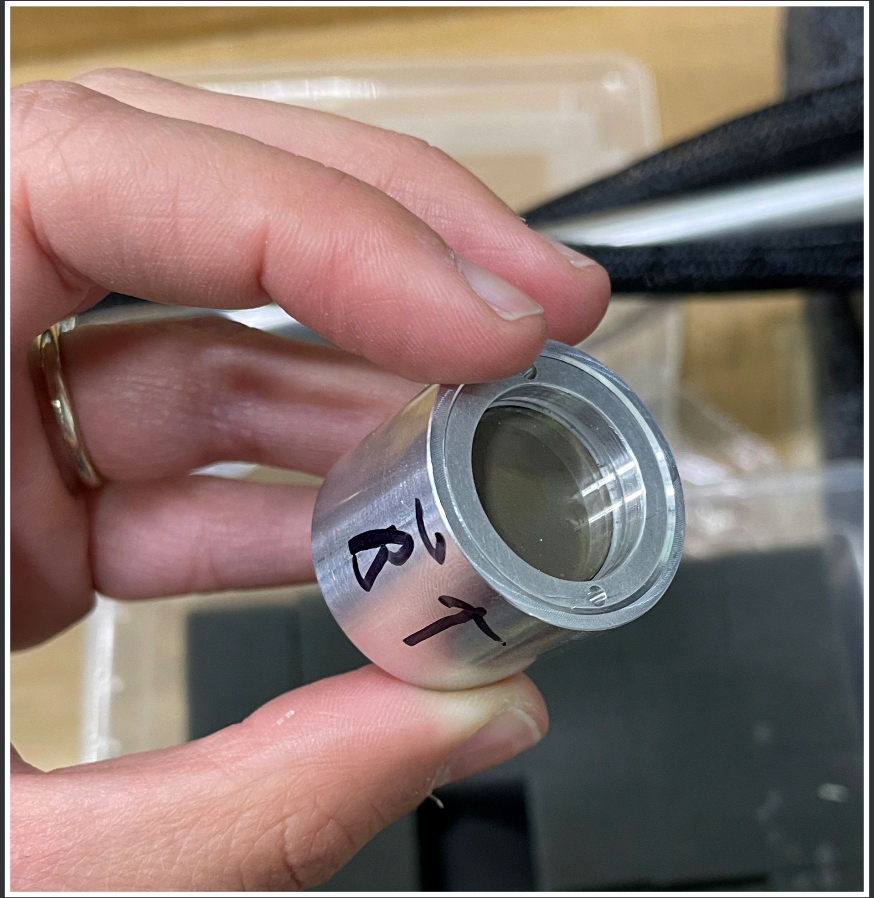

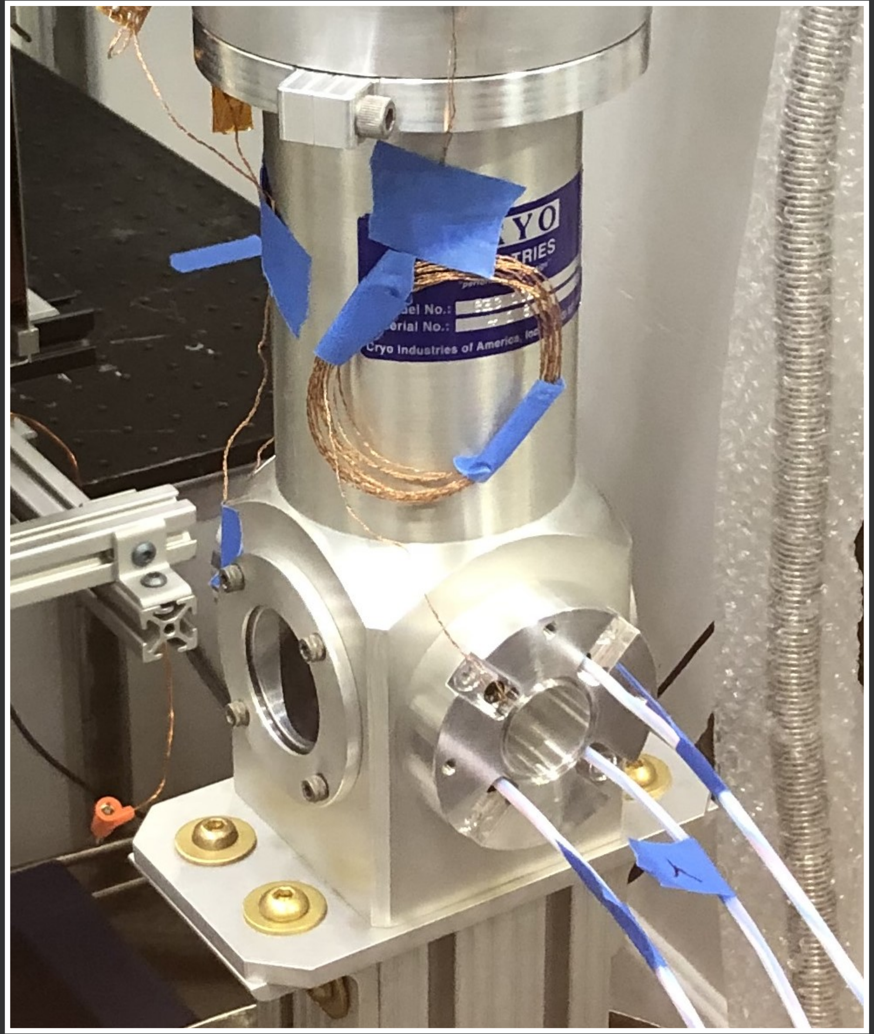

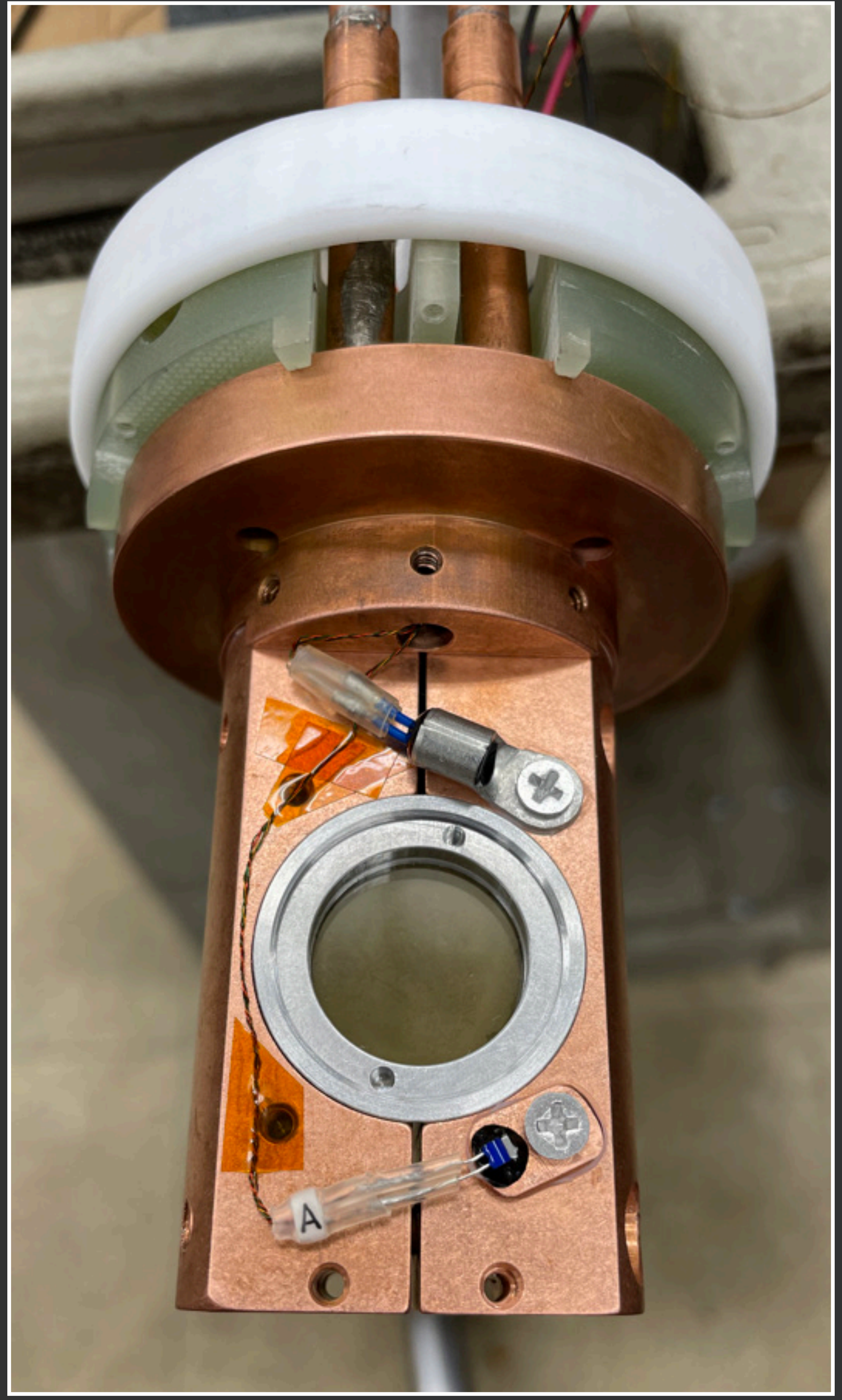

Improvements

Cryostat modification

- all non-mag materials
- "coffin" sample case, better thermal contact
- improved magnetometry, thermometry
- ethylene glycol cooling
- improvement of rotation mechanism

Second layer of mu-metal shielding

- ~100x shielding factor

Upgraded imaging detector

- previously: CCD, ^{6}LiF/ZnS:Cu scintillator, 2048x2048 with 42 μm pixel size
- new: CMOS, GadOx scintillator, 6200x6200 with 16 μm pixel size

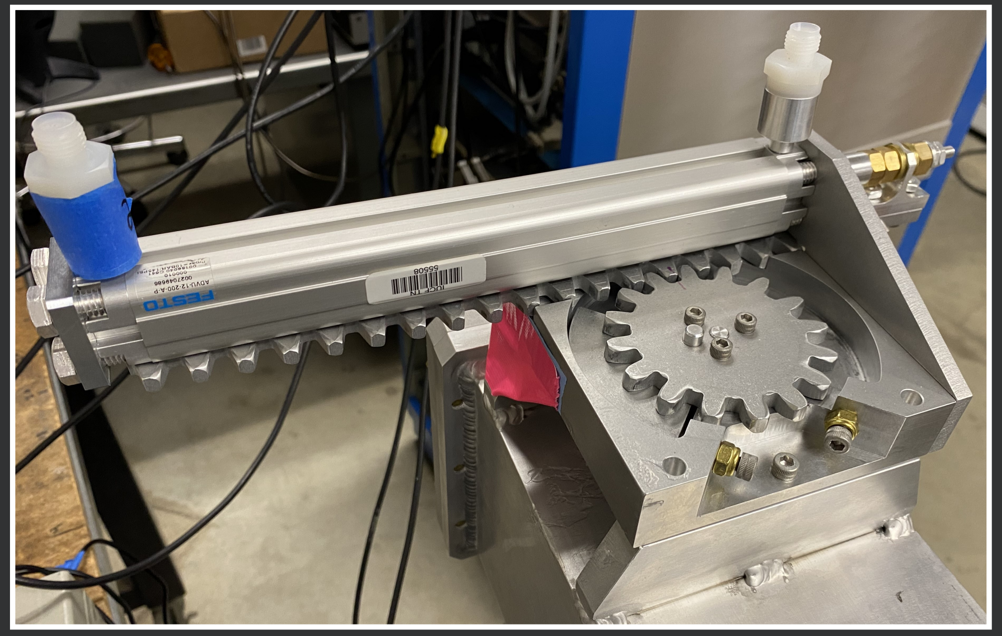

Improvements

Cryostat modification
- all non-mag materials
- "coffin" sample case, better thermal contact
- improved magnetometry, thermometry
- ethylene glycol cooling
- improvement of rotation mechanism

Second layer of mu-metal shielding
- ~100x shielding factor

Upgraded imaging detector
- previously: CCD, ^{6}LiF/ZnS:Cu scintillator, 2048x2048 with 42 μm pixel size
- new: CMOS, GadOx scintillator, 6200x6200 with 16 μm pixel size

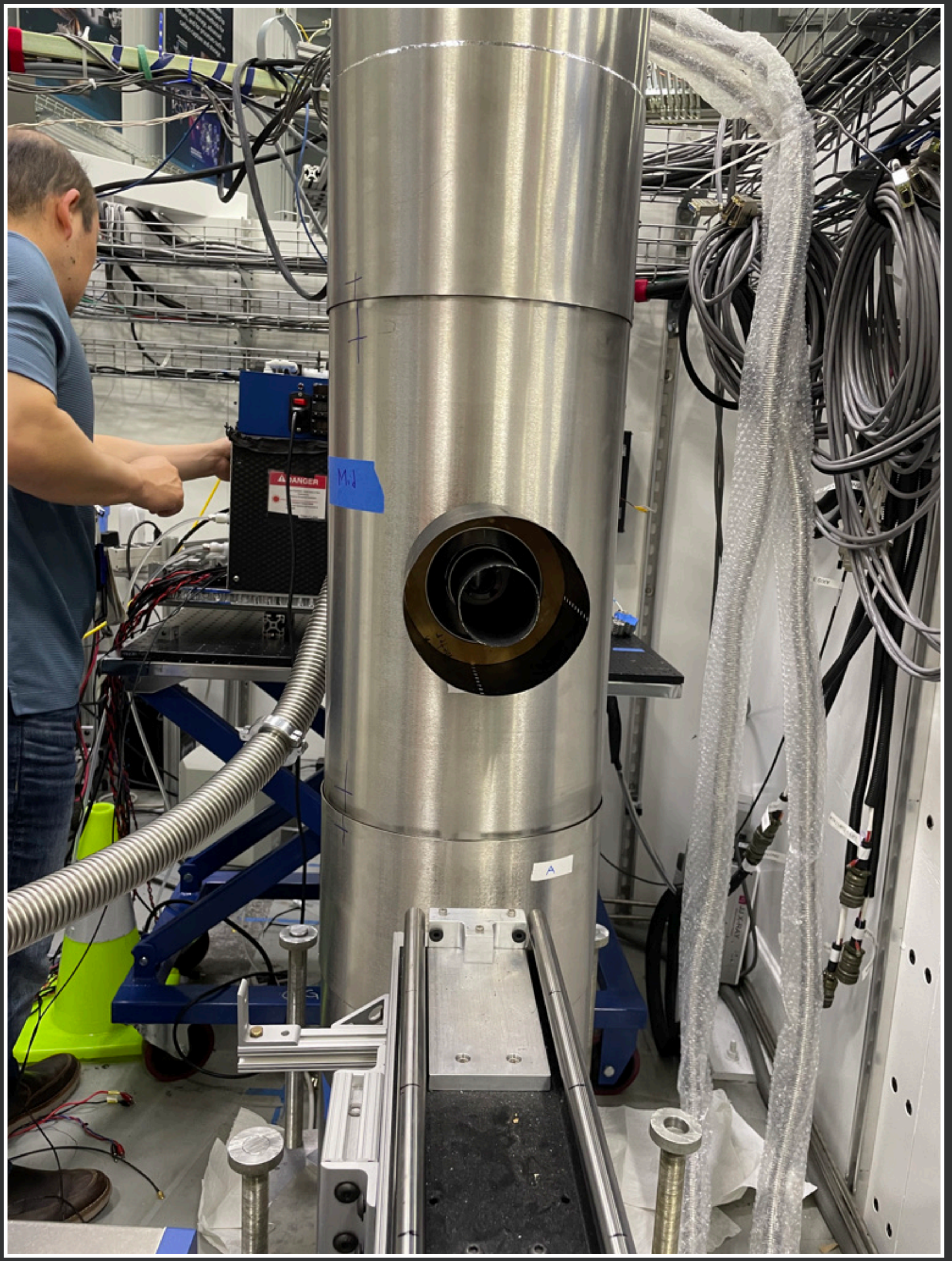

Improvements

Cryostat modification
- all non-mag materials
- "coffin" sample case, better thermal contact
- improved magnetometry, thermometry
- ethylene glycol cooling
- improvement of rotation mechanism

Second layer of mu-metal shielding
- ~100x shielding factor

Upgraded imaging detector
- previously: CCD, ^{6}LiF/ZnS:Cu scintillator, 2048x2048 with 42 μm pixel size
- new: CMOS, GadOx scintillator, 6200x6200 with 16 μm pixel size

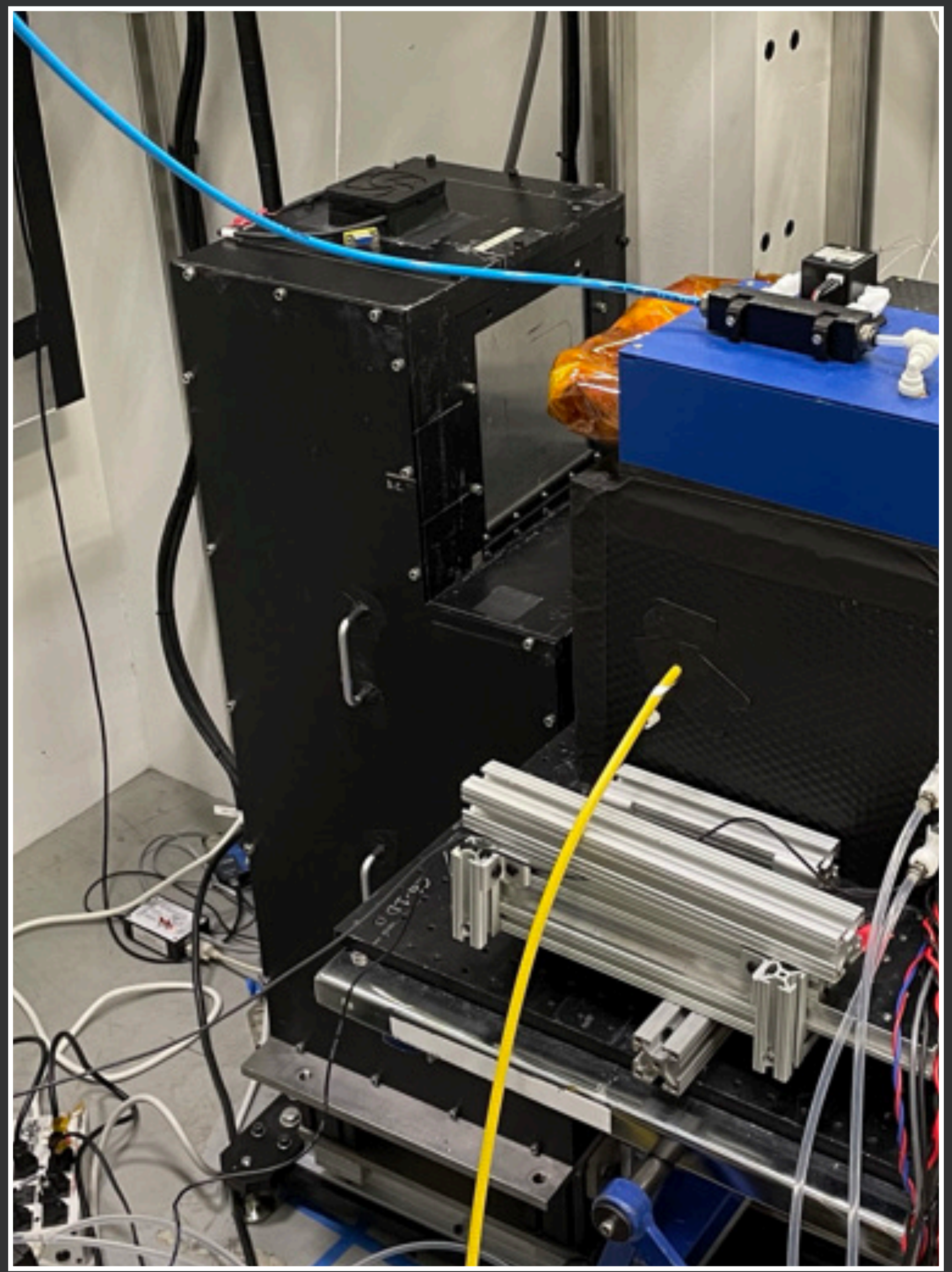

2023

2024

Developments and Future Work

Pre-print on ArXiV, to be submitted very soon to JMMM

Polarized Neutron Measurements of the Internal Magnetization of a Ferrimagnet Across its Compensation Temperature

C. D. Hughes,[1] K. N. Lopez,[1] T. Mulkey,[2] J. C. Long,[3] M. Sarsour,[2] M. Van Meter,[1] S. Samiei,[1] D. V. Baxter,[4] W. M. Snow,[1] L. M. Lommel,[5] Y. Zhang,[6] P. Jiang,[6] E. Stringfellow,[6] P. Zolnierczuk,[6] M. Frost,[6] and M. Odom[6]

[1] *Indiana University/Center for Exploration of Energy and Matter and Indiana University Center for Spacetime Symmetries, 2401 Milo B. Sampson Lane, Bloomington, IN 47408, USA*
[2] *Georgia State University, Atlanta, GA 30303, USA*
[3] *University of Illinois, Urbana, IL 61801-3003, USA*
[4] *Indiana University/Center for Exploration of Energy and Matter, 2401 Milo B. Sampson Lane, Bloomington, IN 47408, USA*
[5] *University of Notre Dame, Holy Cross Dr, Notre Dame, IN 46556, USA*
[6] *Oak Ridge National Laboratory, Oak Ridge, TN 37830, USA*

(Dated: August 28, 2024)

We present the first polarized neutron transmission image of a model Neél ferrimagnetic material, polycrystalline terbium iron garnet ($Tb_3Fe_5O_{12}$, TbIG for short), as it is taken through its compensation temperature T_{comp} where, according to the theory of ferrimagnetism, the internal magnetization should vanish. Our polarized neutron imaging data and the additional supporting measurements using neutron spin echo spectroscopy and SQUID magnetometry are all consistent with a vanishing internal magnetization at T_{comp}.

arXiv:2408.14794v1

Future papers:

- 2024 exotic force constraints
- internal magnetic domain search

MARS 2025A: proposal submitted for transverse electron polarization measurement

SPring-8: Magnetic Compton scattering for absolute electron spin measurement

Development of single-crystal sample

(Shameless Plug of) APS DNP 2024 Ferrimagnets Talks

Katherine Li

Session K10: Fundamental Neutron Physics II
10:30 AM–12:30 PM, Wednesday, October 9, 2024
Hilton Boston Park Plaza Room: Studio 1, Lobby Level

Chair: Jason Fry, Eastern Kentucky University

Abstract: K10.00002 : Slow Neutron Polarimetry for a Spin-Dependent Fifth Force Search in Terbium Iron Garnet: Overview and Neutron Imaging Analysis*
10:42 AM–10:54 AM

Becket Hill

Session J11: Instrumentation III
8:30 AM–9:54 AM, Wednesday, October 9, 2024
Hilton Boston Park Plaza Room: Arlington, Mezzanine Level

Chair: Kay Kolos, Lawrence Livermore National Laboratory

Abstract: J11.00003 : Synthesis and Characterization of Terbium Iron Garnet for the NSR-Ferrimagnets Experiment*
8:54 AM–9:06 AM

Thomas Mulkey

Session K10: Fundamental Neutron Physics II
10:30 AM–12:30 PM, Wednesday, October 9, 2024
Hilton Boston Park Plaza Room: Studio 1, Lobby Level

Chair: Jason Fry, Eastern Kentucky University

Abstract: K10.00003 : Slow Neutron Polarimetry for a Spin-Dependent Fifth Force Search in Terbium Iron Garnet: Advanced Data Analysis Techniques*
10:54 AM–11:06 AM

Michael Van Meter

Session K13: Mini-Symposium: Next Gen Techniques in Fundamental Symmetries and Neutrinos II
10:30 AM–12:06 PM, Wednesday, October 9, 2024
Hilton Boston Park Plaza Room: Statler, Mezzanine Level

Chair: Ronald Fernando Garcia Ruiz, MIT Laboratory for Nuclear Science

Abstract: K13.00003 : Neutron Polarimetric Imaging in Searches for Exotic Spin-Dependent Neutron Interactions with Matter*
10:54 AM–11:06 AM

Krystyna Lopez

Session F10: Fundamental Symmetries II: Beta Decay
2:00 PM–3:36 PM, Tuesday, October 8, 2024
Hilton Boston Park Plaza Room: Studio 1, Lobby Level

Chair: Christopher Morris, Los Alamos National Laboratory

Abstract: F10.00008 : Exploring Exotic Spin-Dependent Interactions via Light Boson Exchange: Theoretical Frameworks and Experimental Techniques in Ferrimagnetic Terbium Iron Garnet*
3:24 PM–3:36 PM

PSTP 2024

20TH INTERNATIONAL WORKSHOP ON POLARIZED SOURCES, TARGETS, AND POLARIMETRY

SEPT. 22-27 | JEFFERSON LAB, NEWPORT NEWS, VA

This work is supported by:

NSF Grants:
PHY-1707986
PHY-2209481

DOE Grant:
DE-SC0010443

GEM Fellowship

INSGC Fellowship

Thank you!

Neutron Spin Rotation—Ferrimagnets Collaboration

Indiana University/CEEM: David Baxter, Caleb Hughes, Katherine Li, Krystyna Lopez, Sepehr Samiei, W. Michael Snow, Michael Van Meter

University of Illinois-Urbana Champaign: Becket Hill, Josh Long

Georgia State University: Thomas Mulkey, Rashmi Parajuli, Murad Sarsour

ORNL-SNS: Matthew Frost, Mary Odom, Piotr Zolnierczuk
ORNL-HFIR: Roger Hobbs, Chenyang Peter Jiang, Erik Stringfellow, James Torres, Yuxuan Zhang

Backup Slides

Synthesis

Co-precipitation method
Combine $RE(NO_3)_3$, $FeCl_3$ and form precipitate with *NaOH*

Synthesis

<u>Co-precipitation method</u>
Combine $RE(NO_3)_3$, $FeCl_3$ and form precipitate with *NaOH*

Wash to neutral, then boil

Synthesis

Co-precipitation method
Combine $RE(NO_3)_3$, $FeCl_3$ and form precipitate with *NaOH*

Wash to neutral, then boil

Dry for 12 hours in furnace

Synthesis

<u>Co-precipitation method</u>

Combine $RE(NO_3)_3$, $FeCl_3$ and form precipitate with *NaOH*

Wash to neutral, then boil

Dry for 12 hours in furnace

Crush into powder

Synthesis

<u>Co-precipitation method</u>
Combine $RE(NO_3)_3$, $FeCl_3$ and form precipitate with *NaOH*

Wash to neutral, then boil

Dry for 12 hours in furnace

Crush into powder

Press into pellets